NEUROSCIENCE
RESEARCH ARTICLE

S. Sánchez-Iglesias et al. / Neuroscience 396 (2019) 119–137

Does Seipin Play a Role in Oxidative Stress Protection and Peroxisome Biogenesis? New Insights from Human Brain Autopsies

Sofía Sánchez-Iglesias,[a] Alberto Fernández-Liste,[b] Cristina Guillín-Amarelle,[a] Alberto Rábano,[c] Leticia Rodriguez-Cañete,[a] Blanca González-Méndez,[a] Antía Fernández-Pombo,[a] Ana Senra[d] and David Araújo-Vilar[a]*

[a] *Thyroid and Metabolic Diseases Unit (U.E.T.eM.), Department of Psychiatry, Radiology, Public Health, Nursing and Medicine (Medicine Area), Center for Research in Molecular Medicine and Chronic Diseases (CIMUS)-IDIS, University of Santiago de Compostela, 15782 Santiago de Compostela, Spain*

[b] *Instituto de Medicina Legal de Galicia (IMELGA), 15707 Santiago de Compostela, A Coruña, Spain*

[c] *Neuropathology Department and Tissue Bank, Fundación CIEN, 28031 Madrid, Spain*

[d] *Department of Physiology, Center for Research in Molecular Medicine and Chronic Diseases (CIMUS)-IDIS, University of Santiago de Compostela, 15782 Santiago de Compostela, Spain*

Abstract—Seipin is a widely expressed protein but with highest levels found in the brain and testes. Seipin function is not yet completely understood, therefore the aim of this study was to evaluate the expression of *BSCL2* transcripts in the central nervous system (CNS) of humans and investigate the effect of their overexpression on a neuron model and their relationship with oxidative stress protection, as well as shed light on the pathogenic mechanisms of Celia's Encephalopathy. We analyzed the expression of *BSCL2* transcripts using real-time RT–PCR in samples across the brain regions of subjects who underwent necropsy and from a case with Celia's Encephalopathy. The transcript encoding the long seipin isoform (*BSCL2*-203, 462 aa) is expressed primarily in the brain and its expression is inversely correlated with age in the temporal lobe, amygdala, and hypothalamus. Strong positive correlations were found between *BSCL2* expression and some genes encoding protective enzymes against oxidative stress including *SOD1* and *SOD2*, as well as peroxisome proliferator-activated receptor gamma (*PPARG*) in the amygdala. These results were experimentally corroborated by overexpressing *BSCL2* transcripts in SH-SY5Y cells with lentiviral transduction and assessing their effects on neuron differentiated cells. Confocal microscopy studies showed that both seipin and PEX16 are closely expressed in the hypothalami of healthy human brains, and PEX16 was absent in the same region of the PELD case. We hypothesize that seipin has specific CNS functions and may play a role in peroxisome biogenesis.

Key words: *BSCL2*, seipin, human brain, peroxisomes, neurodegeneration, lipodystrophy.

INTRODUCTION

The *BSCL2* gene encodes seipin, a resident endoplasmic reticulum (ER) protein with two transmembrane domains, a luminal loop, and two amino and carboxy-terminal tails in the cytoplasm.

The *BSCL2* gene principally encodes three seipin isoforms under natural conditions, 462 (*BSCL2*-203, ENST00000360796.9; CCDS44627), 398 (*BSCL2*-205/207/210, ENST00000403550.5; ENST00000407022.7; ENST00000421906.5; CCDS8031), and 287 (*BSCL2*-201, ENST00000278893.11; CCDS55769) amino acids long, respectively. *BSCL2*-210/207/205 was the first transcript to be described (Magre et al., 2001), and *BSCL2*-203 is the same as *BSCL2*-210/207/205 except for an N-terminal extension of 64 amino acids encoded by exon 1 and part of exon 2. The protein translated from the short transcript is different from the other transcripts, as exon 7 is skipped in *BSCL2*-201 and the reading frame is different from exon 6 to exon 10 (Guillen-Navarro et al., 2013).

In humans, seipin forms 12-unit homoligomers that form a toroid (Sim et al., 2013; Sim et al., 2014). *BSCL2* variants can cause different diseases, such as generalized congenital lipodystrophy type 2 (MIM: # 269700), seipinopathies of first and/or second motor neurons (MIM: # 600794, MIM: # 270685) (Ito and Suzuki, 2009),

*Corresponding author. Address: U.E.T.eM, Department of Psychiatry, Radiology, Public Health, Nursing and Medicine – IDIS, CIMUS, Avda. de Barcelona 3, University of Santiago de Compostela, 15707 Santiago de Compostela, Spain. Fax: +34 981559937.
E-mail address: david.araujo@usc.es (D. Araújo-Vilar).

Abbreviations: CAT, catalase; CNS, central nervous system; ER, endoplasmic reticulum; ET, extraneural tissues; MOI, multiplicity of infection; PBS, phosphate-buffered saline; PELD, Progressive Encephalopathy with or without lipodystrophy; PEX, peroxisomal biogenesis factor; PNS, peripheral nervous system; PPARG, peroxisome proliferator-activated receptor gamma; SOD, superoxide dismutase.

https://doi.org/10.1016/j.neuroscience.2018.11.004
0306-4522/

or Progressive Encephalopathy with or without lipodystrophy, also called Celia's Encephalopathy (PELD, MIM: # 615924) (Guillen-Navarro et al., 2013).

PELD is an infantile neurodegenerative disease with a fatal prognosis before 9 years previously described by our group (Guillen-Navarro et al., 2013). Neurological regression of Celia's Encephalopathy begins at age 3–4, with early signs of severe myoclonic epilepsy, spastic tetraparesis, and severe encephalopathy leading to death before age 9. This disease is extraordinarily rare, and is a consequence of the *BSCL2* gene c.985C > T variant in homozygosis or compound heterozygosis (Alaei et al., 2016; Guillen-Navarro et al., 2013). This variant gives rise to a branch site in exon 7 of the *BSCL2* gene, producing the intronization of that exon leading to an aberrant seipin with a different amino acid sequence than wild-type (*BSCL2*-203) from exon 6 (Guillen-Navarro et al., 2013). The formation of large aberrant seipin macroaggregates leading to ER stress and nuclear accumulation of this abnormal protein are the pathogenetic mechanisms ultimately responsible for Celia's Encephalopathy (Ruiz-Riquelme et al., 2015).

Seipin is a highly evolutionarily conserved protein functioning primarily to modulate the formation of lipid droplets and identified in yeast, *Saccharomyces cerevisiae*, *Caenorhabditis elegans*, zebrafish, fruit fly, and mammals (Cartwright and Goodman, 2012; Salo et al., 2016; Wang et al., 2016). While this gene is mainly expressed in the central nervous system (CNS), pituitary gland, and testis in humans (Guillen-Navarro et al., 2013; Magre et al., 2001), little is known about the function of seipin in the CNS. Recent studies in seipin KO mice have shown a particular action for this protein in the CNS that appears to be mediated by peroxisome proliferator-activated receptor gamma (PPARG) and that influences synaptic transmission primarily through α-amino-3-hydroxy-5-methyl-4-isoxazole propionic acid receptors, and also promotes neuronal differentiation and modulates the behavior and motor skills of these animals (Ebihara et al., 2015; Li et al., 2015; Zhou et al., 2016). Here we evaluate the expression of the various *BSCL2* transcripts across human brain regions and extraneural tissues and investigate the putative functions of seipin in the CNS.

EXPERIMENTAL PROCEDURES

This study was approved by the Ethics Review panel of Xunta de Galicia (Spain) and performed in accordance with the ethical guidelines of the Helsinki Declaration.

Tissue samples

Thirteen post-mortem donors were selected, seven men and six women (aged 21–86 years), primarily deceased by suicide, traffic accident, or natural causes (Table 1) in accordance with the current Spanish legislation, and tissue samples were obtained during autopsy conducted within 24 h of death. Brains were removed and sliced coronally into 12 sections. The frontal cortices in the third slice, parietal and temporal cortices with hippocampi in the seventh slice, occipital lobes in the eleventh, insular cortices, amygdalae, thalami, heads of caudate and putamen nuclei, and cerebellum samples were accurately dissected and collected separately from both cerebral and cerebellar hemispheres, along with the right and left sides of the hypothalamus, mesencephalon, protuberance, and medulla oblongata, as well as the dorsal and ventral spinal cord, anterior pituitary, vagus and trigeminal nerves, skeletal muscles (rectus abdominis and gastrocnemius), adipose tissue from Bichat's fat pad, abdominal subcutaneous tissue, visceral areas and lower limbs, renal cortex and medulla, and liver and gonad samples. These tissues were immediately submerged in liquid nitrogen after removal and subsequently stored at −80 °C until RNA preparation. These dissections yielded a total of 44 tissues for real-time RT–PCR analysis.

RNA extraction and retrotranscription

Total RNA was isolated with the ReliaPrep™ RNA Tissue Miniprep System (Promega, Madrid, Spain). Frozen tissue samples (20 mg of each tissue sample, except for adipose and muscle tissues which required 100 mg) were weighed and then homogenized in 250 μl lysis buffer (LBA previously supplemented with 2% 1-thioglycerol) using a Tissue Ruptor (Qiagen, Hilden, Germany). 750 μl of Trizol reagent (Invitrogen, Madrid, Spain) was added to the homogenized samples, which were then vortexed for 10 s and incubated for 5 min at room temperature to permit complete dissociation of the nucleoprotein complex. Adipose tissue samples required an additional centrifugation step at 12,000*g* for 10 minutes at 4 °C to remove insoluble material, and the fatty layer was removed and discarded while the cleared supernatant was transferred to a new tube. 200 μl of chloroform (Sigma, Madrid, Spain) was then added to the supernatant, which was subsequently shaken vigorously by hand for 15 s and incubated for 2 min at room temperature. This was followed by a centrifugation at 12,000*g* for 15 min at 4 °C, after which the aqueous phase was transferred to a new tube. 35 μl of 2-propanol (Sigma) was added for each 100 μl of supernatant, samples were vortexed for 5 s, and the lysate was transferred to a ReliaPrep column and centrifuged at 14,000*g* for 30 s at room temperature. Subsequent RNA purification was as follows: 200 μl of wash solution was added followed by a centrifugation step at 14,000*g* for 15 s at room temperature; 500 μl of RNA wash solution was added and followed by centrifugation at 14,000*g* for 30 s at room temperature; 300 μl of RNA wash solution was added followed by centrifugation at 20,000*g* for 2 min at room temperature. Finally, RNA was eluted with 30 μl of nuclease and RNase-free water in a last centrifugation step performed at 14,000*g* for 1 min at room temperature. The concentration and purity of each sample was determined by spectrophotometer (ND2000; Nanodrop), and RNA samples were stored at −80 °C until use. The RNA was reverse transcribed using M-MLV reverse transcriptase (Invitrogen), as previously described (Victoria et al., 2010).

Table 1. Demographic and clinical characteristics of subjects

Subjects	Gender	Age	Height (cm)	Weight (kg)
1	Woman	67	165	65
2	Man	73	160	80
3	Man	40	167	75
4	Woman	83	160	90
5	Man	29	184	90
6	Man	61	165	90
7	Man	21	184	80
8	Woman	86	169	69
9	Man	43	178	120
10	Man	43	174	80
11	Woman	21	153	65
12	Woman	66	154	73
13	Woman	77	150	60

Real-time RT–PCR

Specific primers and probes designed by the Universal ProbeLibrary (Roche Diagnostics, Sant Cugat del Valles, Spain) were used in a Light Cycler 2.0 (Roche Diagnostics) to determine the specific expression of the following genes: *CAT*, *NESTIN*, *PEX1*, *PEX11G*, *PEX16*, *PPARG*, *RBFOX3/NeuN*, *SOD1*, *SOD2* (Table 2), and three distinct *BSCL2* transcripts (Fig. 1). Real-time RT–PCR conditions are available upon request. Results were normalized to the *18S* and *RNA polymerase II* genes using the $2^{-\Delta\Delta\ CT}$ method (Livak and Schmittgen, 2001).

Cell culture

The SH-SY5Y neuroblastoma cell line was kindly provided by Dr. Jesús Rodríguez-Requena (Santiago de Compostela, Spain). Undifferentiated cells were maintained in a 1:1 mixture of Ham's F12 (cat. N4888, Sigma–Aldrich) and Minimum Essential Eagle's Medium (cat. M2279, Sigma–Aldrich) supplemented with 15% heat-inactivated fetal bovine serum (cat. 10270-106, Gibco), 1% GlutaMax-I™ (cat. 35050-061, Gibco), 100 units/ml penicillin, 100 μg/ml streptomycin (cat. 15140-122, Gibco), and 1% MEM non-essential amino acids solution (NEAA, cat. 11140050, Gibco). Cells were grown in the presence of 5% CO_2 in a humidified incubator at 37 °C. The cell medium was replaced every 3 days, and the cells were sub-cultured once 90% confluence was reached. The cells were used at early passages (below P17) in all experiments.

Plasmids

A plasmid containing wild-type human seipin fused to a myc tag (6x myc-wt seipin pCS2 + MT) was generously provided by D. Ito (Keio University, Japan), and the myc fused seipin expression plasmid was described previously (Guillen-Navarro et al., 2013). The wild-type lentiviral plasmid was generated as follows: wt seipin cDNA was amplified by PCR using specific primers (forward: 5′-TAAGCAGGTACCTCTTTTTGCAGGATCC CATCGA-3′; reverse: 5′- TAAGCATCTAGAGCCTT GAATTCGCCCTTGAC-3′), then digested with the fast-digest restriction enzymes KpnI and XbaI (cat. FD0524 and FD0684, ThermoFisher Scientific), and purified and inserted into pLenti-CMV-GFP-2A-Puro-Blank (cat. LV073, Applied Biological Materials Inc.) vector. This GFP bicistronic lentiviral plasmid is a replication-

Table 2. Primer sequences and probes

Genes	Forward Primer	Reverse Primer	Probe number	Probe sequence	Amplicon length [nt]
18S	GCAATTATTCCCCATGAACG	GGGACTTAATCAACGCAAGC	48	TTCCCAGT	68
BSCL2 ex1	AGGAGGAAGCTGGGGAAA	CAGCAGCTGGTGGTTCCT	54	CTGGTCTC	78
BSCL2 ex7	TGCGCCTTCATAGGTGTTG	ACCCACTGCATGTAGCTGAA	73	TCCTCAGC	74
BSCL2 ex6-8	AGCGATCATTGAGATCCACA	TTTTCGGATGTTAACCTGAGC	42	CATCCAGC	96
CAT	GGGATCCCATATTGTTTCCAT	ATGTCCGGATCCTTCAGATG	76	TGGCTGTG	76
NESTIN	GAGTTGGGTTCTGGGGAGAT	TCATCCTCCTCGCTCTCTTC	69	CTTCCTCC	77
PEX1	CATTTTCAAAAGCTGATGCTGA	TGCTTGGTTTGAAGTTCTTTCAT	54	CTGGTCTC	88
PEX11G	GCGCTGGAGTCGTACAGG	ACCAGAACTCCACCAACCAG	74	CTGCTGCC	80
PEX16	CCCTCAGTTGCTAAGGGCTAC	CTTCCTGCTTCCGGTCTTAG	73	TCCTCAGC	143
PPARG	GACCTGAAACTTCAAGAGTACCAAA	TGAGGCTTATTGTAGAGCTGAGTC	39	CTCCACCT	95
RBFOX3/NeuN	CCCAACAGAAAGGGCTGAC	CTGGGCTTCCTTCGTCCT	1	CCTGGAGC	68
RPII	GCATCATGAACAGCGATGAG	TCATCCATCTTGTCCACCAC	69	CTTCCTCC	86
SOD1	TCCATGTTCATGAGTTTGGAGAT	TCTGGATAGAGGATTAAAGTGAGGA	40	CAGCAGGC	74
SOD2	GCACTAGCAGCATGTTGAGC	CCGTAGTCGTAGGGCAGGT	1	CCTGGAGC	118

Primer sequences and probes from Universal ProbeLibrary used in qPCR analysis.

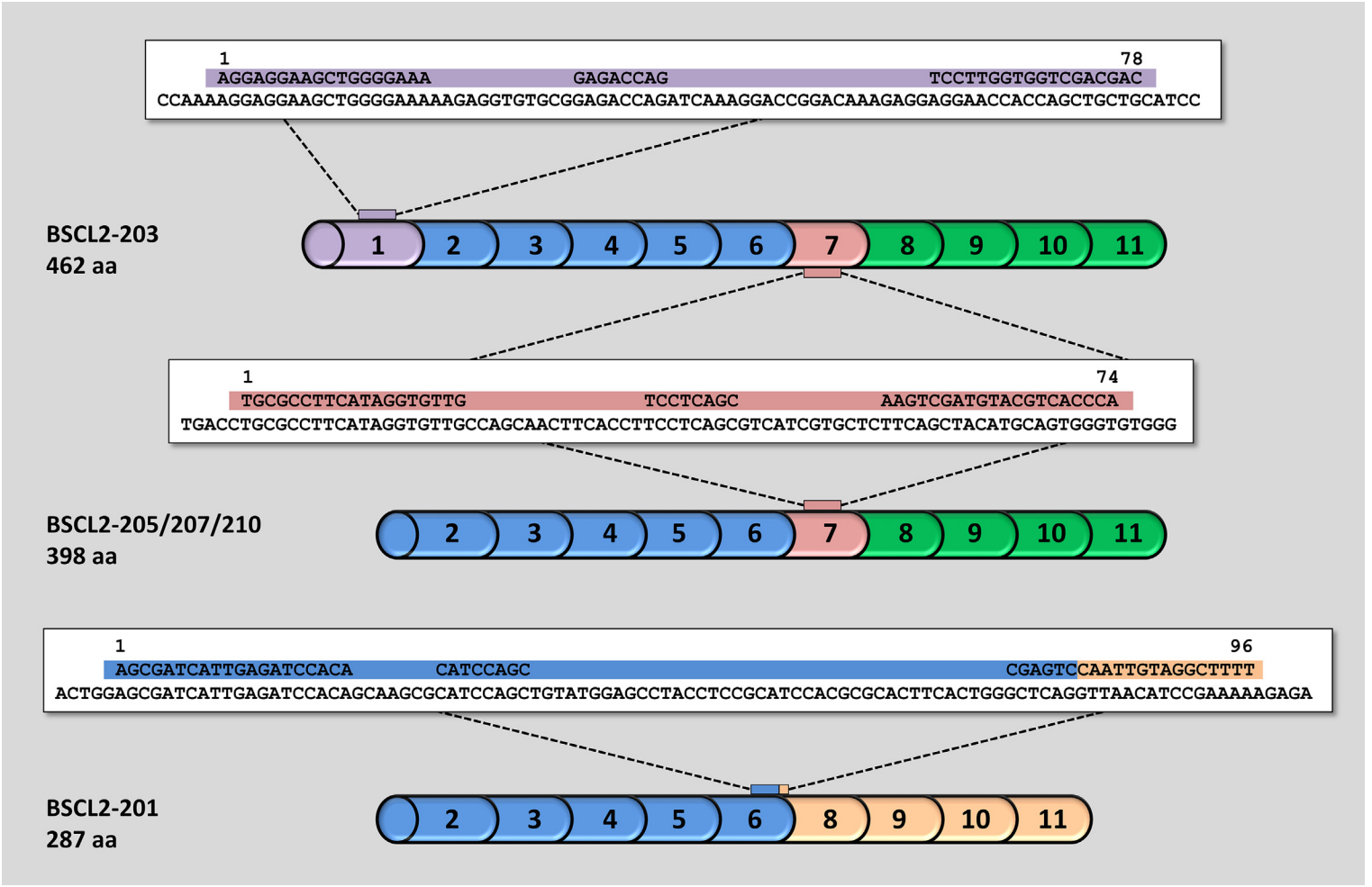

Fig. 1. Three main transcripts of the *BSCL2* gene. The *BSCL2*-203 transcript (ENST00000360796.9; CCDS44627) contains 11 exons coding for a 462-amino-acid-long protein. The *BSCL2*-205/207/210 transcript (ENST00000403550.5; ENST00000407022.7; ENST00000421906.5; CCDS8031) is identical to *BSCL2*-203 except that it lacks the first 192 nucleotides (exon 1 and part of exon 2 of BSCL2-203), resulting in a 398-amino-acid-long protein. The *BSCL2*-201 transcript (ENST00000278893.11; CCDS55769) features exon 7 skipping and generates a protein of 287 amino acids. The probe #73 (TCCTCAGC) used with forward: 5′-TGCGCCTTCATAGGTGTTG-3′ and reverse primer: 5′-ACCCACTGCATGTAGCTGAA-3′ hybridizes with exon 7 of *BSCL2* gen (amplicon 74 nucleotides), while the reverse primer: 5′-AGCGATCATTGAGATCCACA-3′ used with the probe #42 (CATCCAGC) and the forward primer: 5′-TTTTCGGATGTTAACCTGAGC-3′ hybridizes with the union of exon 6 and exon 8 (amplicon 96 nucleotides). The probe #54 (GAGACCAG) used with the forward: 5′-AGGAGGAAGCTGGGGAAA-3′ and the reverse primer: 5′-CAGCAGCTGGTGGTTCCT-3′ (amplicon 78 nucleotides) hybridizes with exon 1 of *BSCL2* gen. Expression of *BSCL2*-203 transcript corresponds to the values obtained from real-time RT–PCR using the probe #54. Expression of *BSCL2*-205/207/210 transcript was calculated by subtracting the values obtained from real-time RT–PCR using probe #73 minus the values obtained from real-time RT–PCR using probe #54. Expression of *BSCL2*-201 transcript corresponds to the values obtained from real-time RT–PCR using probe #42.

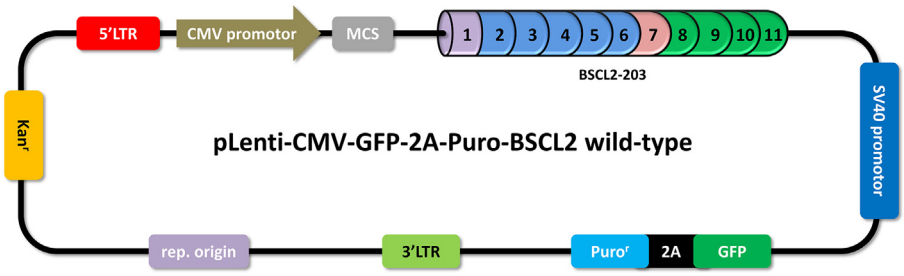

Fig. 2. Lentiviral *BSCL2* plasmid. Plasmid map of lentiviral expression vector used in this study. This pLenti vector includes a CMV promoter for robust and consistent ORF expression, a GFP reporter driven by a separate promoter to the gene of interest to monitor transfection and infection, and a selectable marker expression that confers puromycin resistance.

incompetent third-generation vector, and is depicted in Fig. 2. Full sequences were confirmed by sequencing.

Lentiviral transduction

Cells were seeded into 6-well plates (cat. 3516, Corning, Costar) at a density of 5000 cells per cm^2. The medium was removed twenty-four hours after seeding and the cells were washed with phosphate-buffered saline (PBS). Viral particles (wild-type seipin), and the empty vector as a control, all with functional titers $>10^9$ transducing units/ml produced by Cyagen Biosciences (Guangzhou, China) were added at a multiplicity of infection (MOI) of 200 viral particles/cell to a serum-free medium in the presence of Lentiblast A/B (1:100/1:1000, Oz Biosciences, Marseille, France). Serum was added 4 hours after initial infection (final infection volume 1 ml), the medium was removed twenty-four hours after infection, and the cells were washed with phosphate-buffered saline (PBS). Cells were then cultured with typical SH-SY5Y medium and puromycin dihydrochloride (2 μg/ml final concentration, cat. P8833, Sigma–Aldrich) was subsequently added to the cell culture medium every 2–3 days until resistant stable cells were formed. Cells were then routinely grown as described above.

Differentiation

Stably transfected cells were seeded into six-well plates at density of 10,000 cells per cm^2 and allowed to adhere for 2 days. Pre-differentiation was then started in DMEM high glucose (D5796, Sigma–Aldrich) supplemented with 3% heat-inactivated fetal bovine serum, 100 units/ml penicillin, and 100 μg/ml streptomycin with 10 μM retinoic acid (cat. R2625, Sigma–Aldrich), freshly prepared in DMSO and kept in the dark. Undifferentiated cells were cultured in identical medium without retinoic acid. The second phase of differentiation was initiated after 3 days in these conditions (day 4) with Neurobasal medium (cat. 21103-049, Gibco), 50 ng/ml BDNF (cat. 450-02, Peprotech), 1 mM dibutyryl-cAMP (cat. sc-201567A, Santa Cruz), 20 mM KCl (cat. 131494, Panreac), 10 μM retinoic acid, 1% B27 (cat. 17504-044, Gibco), 1% Glutamax 100×, 1% N-2 supplement (cat. 17502-048, Gibco), 100 units/ml penicillin, and 100 μg/ml streptomycin. Undifferentiated cells were maintained in high glucose DMEM, supplemented with 1% heat-inactivated fetal bovine serum, 100 units/ml penicillin, and 100 μg/ml streptomycin. The culture medium was changed every 2 days and supplemented with fresh additives. Differences in cell morphology between proliferative and differentiated cells were evaluated under phase contrast light microscopy with an Olympus IX51 microscope (Olympus Corporation, Tokyo, Japan) and photographed with an Olympus DP72 digital camera using the cellSens software (Olympus Corporation). Cells were harvested on day 8.

Immunostaining

The hypothalamus of the homozygous index case c.985C > T and of two control cases (male and female, 59 and 75 years at death, respectively) were fixed previously with 10% neutral buffered formalin (Bio-Optica, cat. 05-K01022) for 24 h at room temperature and embedded in paraffin. After deparaffinization and rehydration, slides were pre-treated with PT-link (Dako, California, USA) for 20 min at 95 °C in Tris/EDTA buffer, pH 9. Slides were then washed four times with PBS and incubated with 1:250 anti PEX16 antibody (Santa Cruz Biotechnology) and 1:125 anti-seipin antibody HPA042394 (Sigma–Aldrich, The Human Protein Atlas) overnight at 4 °C. The next day, the slides were washed four times with PBS and incubated with Alexa Fluor 555 (Thermo-Fisher Scientific, cat. A31572) conjugated anti-mouse secondary antibody, and Alexa Fluor 488 (Thermo-Fisher Scientific, cat. A21202) conjugated anti-rabbit secondary antibody for 1 h in darkness, washed with double-distilled water. Slides were then treated to quench autofluorescence background with 0.1% Sudan Black B (Sigma, cat. 199664) in 70% ethanol for less than 5 min at room temperature and washed three times, for 5 min each with double-distilled water. Finally, they were mounted in aqueous medium containing 1:1000 DAPI (Sigma–Aldrich, cat. D9542).

Confocal fluorescence microscopy

Immunofluorescence staining was assessed with a Leica TCS SP2 confocal microscope using a HCX PL APO 63×/1.3 glycerol-immersion objective and Leica Confocal Software (Leica Microsystems Heidelberg GmbH, Mannheim, Germany). Images were obtained by a sequential scan method and three different laser lines to avoid simultaneous excitation and possible overlap. Confocal acquisition of the fluorescence labels was performed as follows: DAPI, color-coded in blue (Blue-Diode, excited at 405 nm and recorded on 425–470 nm), Alexa Fluor 488 nm, color-coded in green (Argon laser, excited at 488 nm and recorded at 500–555 nm), and Alexa Fluor 555 nm, color-coded in red

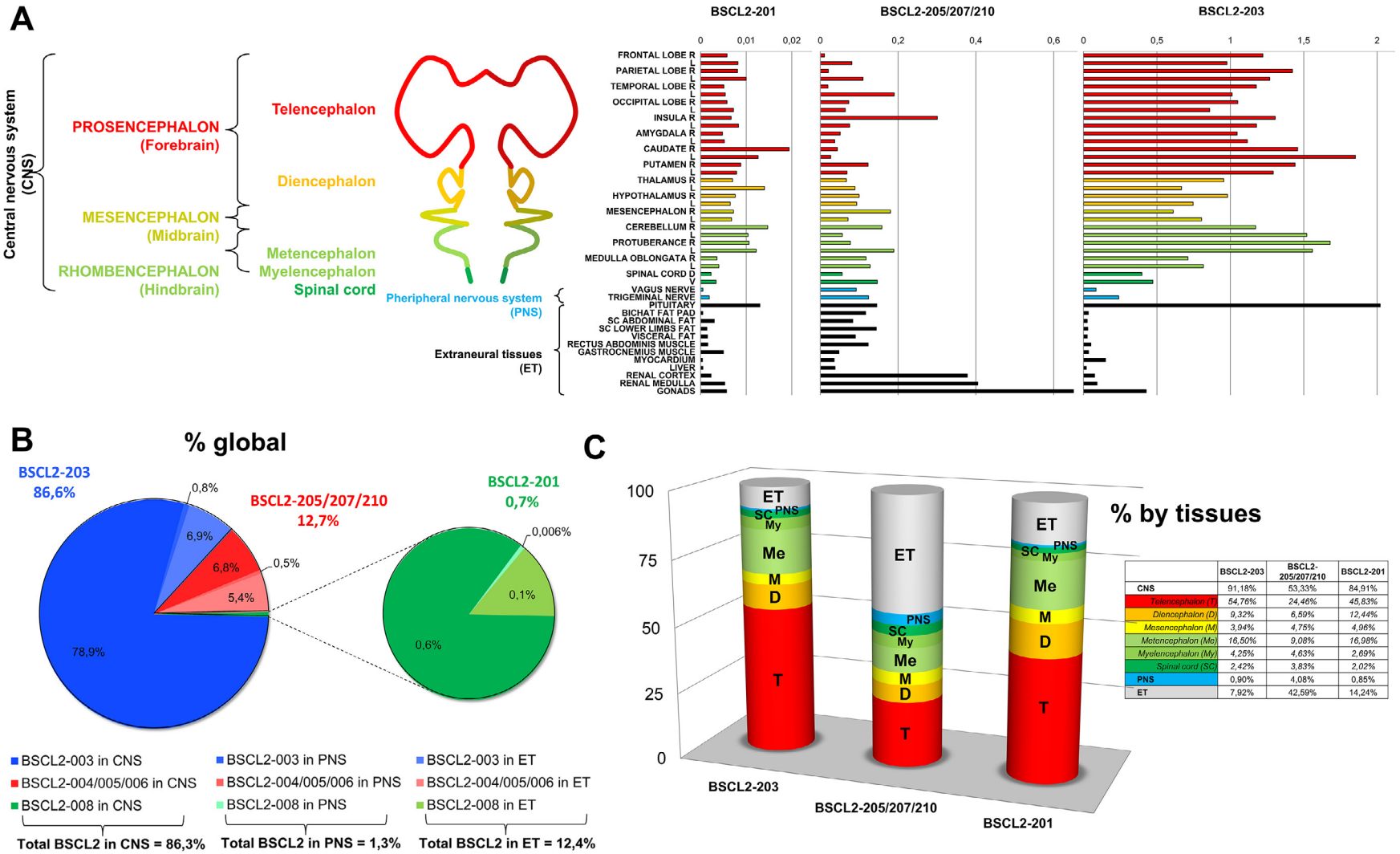

	BSCL2-203	BSCL2-205/207/210	BSCL2-201
CNS	91,18%	53,33%	84,91%
Telencephalon (T)	*54,76%*	*24,46%*	*45,83%*
Diencephalon (D)	*9,32%*	*6,59%*	*12,44%*
Mesencephalon (M)	*3,94%*	*4,75%*	*4,96%*
Metencephalon (Me)	*16,50%*	*9,08%*	*16,98%*
Myelencephalon (My)	*4,25%*	*4,63%*	*2,69%*
Spinal cord (SC)	*2,42%*	*3,83%*	*2,02%*
PNS	0,90%	4,08%	0,85%
ET	7,92%	42,59%	14,24%

Fig. 3. *BSCL2* transcripts' expression. (A) Summary of the relative expression of the three *BSCL2* transcripts across the primary brain divisions, the peripheral nervous system (PNS), and the extraneural tissues (ET). Details are available in Table 3. (B) Percent expression of *BSCL2* transcripts in CNS, PNS and ET. *BSCL2*-203 (blue), *BSCL2*-205/207/210 (red), and *BSCL2*-201 (green) expression are referred to as *BSCL2* total expression. (C) Percentage expression of *BSCL2* transcripts in primary brain divisions: telencephalon (T), diencephalon (D), mesencephalon (M), metencephalon (Me), myelencephalon (My), spinal cord (SC); peripheral nervous system (PNS) and extraneural tissues (ET). All samples were analyzed in duplicate, $n = 13$. All results were normalized to the *18S* gene.

(DPS diode, excited at 561 nm and recorded at 581–675 nm). Two random visual fields were analyzed for each group.

Statistical analysis

Real-time PCR analyses were done by duplicates, and statistical significance was determined using a non-parametric Kruskal–Wallis test followed by a Mann–Whitney U post-hoc with Bonferroni's correction. Correlations were tested using the Spearman R correlation coefficient and partial correlations were utilized to correlate two variables while adjusting for other one. Data are presented as mean ± SD with statistical significance set at $p < 0.05$. All statistical analyses were performed using SPSS for Mac (release 22.0; SPSS, Chicago, IL, USA).

RESULTS

Patterns of *BSCL2* expression in human tissues

We evaluated the relative expression of seipin transcripts in the CNS, the peripheral nervous system (PNS), and extraneural tissues (ET) in 13 subjects (Fig. 3A, detailed with significance in Table 3). The total expression of *BSCL2* was 6.9 times higher in the CNS than in any of the other tissues ($p < 0.001$): 86.3% in CNS, 1.3% in

Table 3. Relative expression of *BSCL2* transcripts

#	Tissues	*BSCL2*-203	*BSCL2*-205/207/210	*BSCL2*-201
1	Frontal Lobe R	1.222 ± 0.723$^{*,\#}$	0.0107 ± 0.0375*	0.0058 ± 0.00379$^{\#}$
2	Frontal lobe L	0.977 ± 0.799$^{*,\#}$	0.0812 ± 0.160*	0.0082 ± 0.0077$^{\#}$
3	Parietal lobe R	1.423 ± 0.827$^{*,\#}$	0.0206 ± 0.059*,§	0.0081 ± 0.005$^{\#,\S}$
4	Parietal lobe L	1.269 ± 0.895$^{*,\#}$	0.110 ± 0.159*,§	0.01 ± 0.0082$^{\#,\S}$
5	Temporal lobe R	1.177 ± 0.709$^{*,\#}$	0.0197 ± 0.041*,§	0.0051 ± 0.0029$^{\#,\S}$
6	Temporal lobe L	1.012 ± 0.574$^{*,\#}$	0.19 ± 0.199*,§	0.0054 ± 0.0036$^{\#,\S}$
7	Occipital lobe R	1.051 ± 0.820$^{*,\#}$	0.0732 ± 0.240*,§	0.0058 ± 0.0053$^{\#,\S}$
8	Occipital lobe L	0.859 ± 0.775$^{*,\#}$	0.0642 ± 0.127*,§	0.0072 ± 0.0053$^{\#,\S}$
9	Insula R	1.306 ± 0.905$^{*,\#}$	0.301 ± 0.305*,§	0.0067 ± 0.004$^{\#,\S}$
10	Insula L	1.178 ± 0.680$^{*,\#}$	0.0756 ± 0.084*,§	0.0083 ± 0.0073$^{\#,\S}$
11	Amygdala R	1.046 ± 0.643$^{*,\#}$	0.0511 ± 0.066*,§	0.0048 ± 0.0032$^{\#,\S}$
12	Amygdala L	1.116 ± 0.744$^{*,\#}$	0.037 ± 0.079*,§	0.0052 ± 0.0033$^{\#,\S}$
13	Thalamus R	0.955 ± 0.521$^{*,\#}$	0.0669 ± 0.0830*,§	0.007 ± 0.0059$^{\#,\S}$
14	Thalamus L	0.667 ± 0.448$^{*,\#}$	0.0889 ± 0.071*,§	0.014 ± 0.022$^{\#,\S}$
15	Caudate R	1.459 ± 0.729$^{*,\#}$	0.044 ± 0.094*	0.0194 ± 0.0178$^{\#}$
16	Caudate L	1.852 ± 0.933$^{*,\#}$	0.0268 ± 0.0760*	0.0126 ± 0.0076$^{\#}$
17	Putamen R	1.441 ± 0.660$^{*,\#}$	0.1228 ± 0.1841*,§	0.0088 ± 0.0047$^{\#,\S}$
18	Putamen L	1.292 ± 0.520$^{*,\#}$	0.0686 ± 0.198*,§	0.0079 ± 0.0039$^{\#,\S}$
19	Hypothalamus R	0.981 ± 0.645$^{*,\#}$	0.1 ± 0.1449*,§	0.0076 ± 0.0056$^{\#,\S}$
20	Hypothalamus L	0.746 ± 0.461$^{*,\#}$	0.0937 ± 0.083*,§	0.0065 ± 0.0054$^{\#,\S}$
21	Pituitary	2.021 ± 0.716$^{*,\#}$	0.1451 ± 0.214*,§	0.0130 ± 0.0055$^{\#,\S}$
22	Cerebellum R	1.172 ± 0.793$^{*,\#}$	0.1584 ± 0.427*,§	0.0147 ± 0.0192$^{\#,\S}$
23	Cerebellum L	1.521 ± 0.879$^{*,\#}$	0.0566 ± 0.1220*	0.0104 ± 0.0074$^{\#}$
24	Mesencephalon R	0.611 ± 0.524$^{*,\#}$	0.1804 ± 0.126*,§	0.0072 ± 0.0066$^{\#,\S}$
25	Mesencephalon L	0.804 ± 0.777$^{*,\#}$	0.07126 ± 0.0928*,§	0.0068 ± 0.0066$^{\#,\S}$
26	Protuberance R	1.680 ± 1.022$^{*,\#}$	0.0773 ± 0.197*,§	0.0106 ± 0.0068$^{\#,\S}$
27	Protuberance L	1.559 ± 0.932$^{*,\#}$	0.189 ± 0.290*,§	0.0122 ± 0.0088$^{\#,\S}$
28	Medulla oblongata R	0.711 ± 0.554$^{*,\#}$	0.1176 ± 0.151*,§	0.00358 ± 0.0035$^{\#,\S}$
29	Medulla oblongata L	0.816 ± 0.620$^{*,\#}$	0.128 ± 0.1324*,§	0.004 ± 0.0041$^{\#,\S}$
30	Spinal cord D	0.397 ± 0.275$^{*,\#}$	0.0561 ± 0.050*,§	0.0023 ± 0.0023$^{\#,\S}$
31	Spinal cord V	0.472 ± 0.405$^{*,\#}$	0.1467 ± 0.086*,§	0.0034 ± 0.0024$^{\#,\S}$
32	Bichat fat pad	0.033 ± 0.008$^{*,\#}$	0.1165 ± 0.052*,§	0.00048 ± 0.00023$^{\#,\S}$
33	SC abdominal fat	0.025 ± 0.026$^{*,\#}$	0.0836 ± 0.041*,§	0.003 ± 0.0029$^{\#,\S}$
34	SC L.L. fat	0.029 ± 0.012$^{*,\#}$	0.144 ± 0.054*,§	0.0014 ± 0.0007$^{\#,\S}$
35	Visceral fat	0.025 ± 0.013$^{\#}$	0.09 ± 0.074§	0.0015 ± 0.00097$^{\#,\S}$
36	Rectus abdominis muscle	0.050 ± 0.015$^{*,\#}$	0.123 ± 0.0709*,§	0.00159 ± 0.00079$^{\#,\S}$
37	Gastrocnemius muscle	0.034 ± 0.016$^{\#}$	0.0479 ± 0.045§	0.005 ± 0.0092$^{\#,\S}$
38	Myocardium	0.015 ± 0.006$^{*,\#}$	0.0357 ± 0.0165*,§	0.0004 ± 0.0002$^{\#,\S}$
39	Liver	0.019 ± 0.009$^{*,\#}$	0.038 ± 0.0227*,§	0.0005 ± 0.00032$^{\#,\S}$
40	Vagus nerve	0.085 ± 0.035$^{\#}$	0.0924 ± 0.041§	0.0005 ± 0.0002$^{\#,\S}$
41	Trigeminal nerve	0.239 ± 0.144$^{*,\#}$	0.1239 ± 0.097*,§	0.0019 ± 0.0016$^{\#,\S}$
42	Renal cortex	0.075 ± 0.023$^{\#}$	0.378 ± 0.786§	0.0023 ± 0.0018$^{\#,\S}$
43	Renal medulla	0.092 ± 0.051$^{*,\#}$	0.4049 ± 0.507*,§	0.0053 ± 0.0049$^{\#,\S}$
44	Gonads	0.427 ± 0.456$^{\#}$	0.651 ± 0.647§	0.0057 ± 0.0044$^{\#,\S}$

Relative expression of the three *BSCL2* transcripts in encephalic and non-encephalic post-mortem tissues. $^{*}p < 0.05$, *BSCL2*-203 transcript referred to *BSCL2*-205/207/210 transcripts; $^{\#}p < 0.05$, *BSCL2*-203 transcript referred to *BSCL2*-201 transcript; $^{\S}p < 0.05$, *BSCL2*-205/207/210 transcripts referred to *BSCL2*-201 transcript. All samples were analyzed in duplicate, $n = 13$. Results were normalized for the *18S* gene. R: right, L: left, V: ventral, D: dorsal, L.L.: lower limbs, SC: subcutaneous.

Table 4. *BSCL2* transcripts expression in men and women

Tissues	Side	*BSCL2*-203			*BSCL2*-205/207/210			*BSCL2*-201		
		Male (n = 7)	Female (n = 6)	Δ%	Male (n = 7)	Female (n = 6)	Δ%	Male (n = 7)	Female (n = 6)	Δ%
Frontal lobe	R	1.27 ± 0.83	1.17 ± 0.62		0.02 ± 0.05	0		0.006 ± 0.005	0.005 ± 0.002	
	L	1.14 ± 0.87	0.79 ± 0.69		0.045 ± 0.14*	0.124 ± 0.177	−63	0.0089 ± 0.005	0.0074 ± 0.01	
Parietal lobe	R	1.27 ± 0.93	1.59 ± 0.68		0.028 ± 0.078	0.012 ± 0.029		0.0066 ± 0.0053	0.0099 ± 0.0044	
	L	1.12 ± 0.93	1.44 ± 0.85		0.074 ± 0.108	0.15 ± 0.20		0.0086 ± 0.0084	0.0126 ± 0.0078	
Temporal lobe	R	1.41 ± 0.74*	0.899 ± 0.58	+57	0.023 ± 0.045	0.016 ± 0.038		0.0058 ± 0.0028	0.0044 ± 0.0030	
	L	1.185 ± 0.6*	0.81 ± 0.49	+46	0.30 ± 0.20*	0.059 ± 0.096	+408	0.0062 ± 0.0037	0.0045 ± 0.0035	
Occipital lobe	R	0.92 ± 0.7	1.2 ± 0.95		0.009 ± 0.024	0.15 ± 0.35		0.0041 ± 0.0024	0.0080 ± 0.0070	
	L	0.69 ± 0.58	1.06 ± 0.94		0.036 ± 0.037	0.097 ± 0.18		0.0072 ± 0.0061	0.0072 ± 0.0046	
Insula	R	1.51 ± 0.91	1.07 ± 0.88		0.40 ± 0.35	0.19 ± 0.20		0.0071 ± 0.0031	0.0059 ± 0.0049	
	L	1.18 ± 0.67	1.17 ± 0.73		0.109 ± 0.087*	0.037 ± 0.064	+194	0.0087 ± 0.0077	0.0080 ± 0.0072	
Amygdala	R	1.24 ± 0.62	0.77 ± 0.60		0.067 ± 0.078	0.029 ± 0.038		0.0056 ± 0.0034	0.0039 ± 0.0028	
	L	1.39 ± 0.73	0.73 ± 0.59		0.034 ± 0.058	0.42 ± 0.11		0.0057 ± 0.0032	0.0046 ± 0.0036	
Thalamus	R	1.03 ± 0.49	0.87 ± 0.57		0.065 ± 0.086	0.069 ± 0.083		0.0084 ± 0.0072	0.0056 ± 0.0040	
	L	0.63 ± 0.36	0.71 ± 0.55		0.12 ± 0.056	0.05 ± 0.07		0.0189 ± 0.0289	0.0083 ± 0.0079	
Caudate	R	1.59 ± 0.56	1.31 ± 0.89		0.042 ± 0.094	0.047 ± 0.099		0.0158 ± 0.0143	0.0238 ± 0.0212	
	L	2.24 ± 0.95	1.40 ± 0.70		0.018 ± 0.048	0.037 ± 0.1		0.0139 ± 0.0058	0.0112 ± 0.0095	
Putamen	R	1.65 ± 0.66	1.2 ± 0.59		0.149 ± 0.208	0.093 ± 0.156		0.0098 ± 0.0044	0.0078 ± 0.0052	
	L	1.29 ± 0.51	1.30 ± 0.56		0.02 ± 0.03	0.125 ± 0.287		0.0075 ± 0.0037	0.0084 ± 0.0044	
Hypothalamus	R	0.97 ± 0.56	1.0 ± 0.76		0.108 ± 0.13	0.091 ± 0.166		0.0072 ± 0.0048	0.0083 ± 0.0067	
	L	0.87 ± 0.46	0.61 ± 0.43		0.13 ± 0.066*	0.051 ± 0.084	+155	0.0080 ± 0.0064	0.0049 ± 0.0035	
Pituitary		1.97 ± 0.79	2.08 ± 0.66		0.193 ± 0.270	0.089 ± 0.11		0.0099 ± 0.0037*	0.0166 ± 0.0052	−40
Cerebellum	R	0.94 ± 0.80	1.44 ± 0.72		0.077 ± 0.13	0.25 ± 0.61		0.0076 ± 0.0067*	0.0230 ± 0.0255	−67
	L	1.53 ± 0.84	1.51 ± 0.97		0.07 ± 0.155	0.042 ± 0.071		0.0116 ± 0.0090	0.0091 ± 0.0052	
Mesencephalon	R	0.53 ± 0.52	0.71 ± 0.53		0.198 ± 0.142	0.16 ± 0.11		0.0062 ± 0.0073	0.0084 ± 0.0059	
	L	0.90 ± 0.90	0.69 ± 0.63		0.066 ± 0.09	0.078 ± 0.099		0.0074 ± 0.0075	0.0062 ± 0.0058	
Protuberance	R	1.99 ± 0.95	1.32 ± 1.03		0.121 ± 0.256	0.027 ± 0.077		0.0123 ± 0.0071	0.0087 ± 0.0063	
	L	1.7 ± 0.75	1.39 ± 1.12		0.17 ± 0.17	0.21 ± 0.39		0.0140 ± 0.0090	0.0103 ± 0.0086	
Medulla oblongata	R	0.83 ± 0.63	0.54 ± 0.41		0.153 ± 0.156	0.076 ± 0.139		0.0043 ± 0.0044	0.0027 ± 0.0019	
	L	0.96 ± 0.64	0.64 ± 0.57		0.168 ± 0.16	0.084 ± 0.074		0.0051 ± 0.0049	0.0028 ± 0.0025	
Spinal cord	D	0.42 ± 0.32	0.37 ± 0.22		0.070 ± 0.052	0.040 ± 0.044		0.0017 ± 0.0009	0.0031 ± 0.0032	
	V	0.66 ± 0.46*	0.25 ± 0.17	+164	0.182 ± 0.088*	0.106 ± 0.066	+71	0.0044 ± 0.0027	0.0023 ± 0.0016	
Bichat fat pad	–	0.034 ± 0.010	0.033 ± 0.008		0.135 ± 0.054	0.095 ± 0.053		0.0004 ± 0.0002	0.0006 ± 0.0003	
SC abdominal fat	–	0.034 ± 0.034	0.016 ± 0.003		0.10 ± 0.047*	0.059 ± 0.012	+69	0.0032 ± 0.0033	0.0028 ± 0.0026	
SC lower limbs fat	–	0.029 ± 0.009	0.030 ± 0.015		0.145 ± 0.042	0.144 ± 0.068		0.0016 ± 0.0007	0.0012 ± 0.0007	
Visceral fat	–	0.030 ± 0.013*	0.020 ± 0.013	−33	0.091 ± 0.028	0.090 ± 0.11		0.0012 ± 0.0007	0.0019 ± 0.0011	
Rectus abdominis muscle	–	0.047 ± 0.019	0.054 ± 0.008		0.092 ± 0.039*	0.16 ± 0.08	−42	0.0016 ± 0.0009	0.0016 ± 0.0007	
Gastrocnemius muscle	–	0.034 ± 0.016	0.035 ± 0.019		0.056 ± 0.056	0.039 ± 0.030		0.0031 ± 0.0051	0.0073 ± 0.0123	
Myocardium	–	0.016 ± 0.009	0.014 ± 0.003		0.037 ± 0.01	0.035 ± 0.022		0.0005 ± 0.0002	0.0004 ± 0.0002	
Liver	–	0.021 ± 0.01	0.018 ± 0.009		0.041 ± 0.022	0.036 ± 0.024		0.0005 ± 0.0004	0.0005 ± 0.0003	
Vagus nerve	–	0.10 ± 0.03*	0.07 ± 0.03	+43	0.117 ± 0.032*	0.064 ± 0.031	+83	0.0005 ± 0.0002	0.0006 ± 0.0003	
Trigeminal nerve	–	0.25 ± 0.18	0.23 ± 0.09		0.16 ± 0.10*	0.077 ± 0.070	+108	0.0021 ± 0.0019	0.0017 ± 0.0013	
Renal cortex	–	0.085 ± 0.026	0.064 ± 0.014		0.57 ± 1.05	0.16 ± 0.052		0.0029 ± 0.0023	0.0018 ± 0.0009	
Renal medulla	–	0.089 ± 0.053	0.096 ± 0.051		0.42 ± 0.56	0.39 ± 0.46		0.0037 ± 0.0025	0.0072 ± 0.0064	
Gonads	–	0.51 ± 0.14*	0.33 ± 0.66	+54	1.17 ± 0.42*	0.044 ± 0.051	+2559	0.0089 ± 0.0030*	0.0020 ± 0.003	+345

Relative expression of the encephalic and non-encephalic post-mortem tissues in female and male subjects, $^{*}p < 0.05$. All samples were analyzed in duplicate, n = 13. Results were normalized for the *18S* gene.

Table 5. *BSCL2* transcripts expression in young and old subjects (median age 61 years)

Tissues	Side	*BSCL2*-203			*BSCL2*-205/207/210			*BSCL2*-201		
		<61 y. (n = 6)	≥61 y. (n = 7)	Δ%	<61 y. (n = 6)	≥61 y. (n = 7)	Δ%	<61 y. (n = 6)	≥61 y. (n = 7)	Δ%
Frontal lobe	R	1.68 ± 0.69*	0.83 ± 0.49	−51	0.023 ± 0.053	0.0003 ± 0.001		0.0079 ± 0.004*	0.004 ± 0.0025	−49
	L	0.99 ± 0.72	0.96 ± 0.89		0.07 ± 0.18	0.088 ± 0.15		0.009 ± 0.0049	0.0075 ± 0.0096	
Parietal lobe	R	1.71 ± 0.76	1.18 ± 0.83		0.03 ± 0.08	0.012 ± 0.03		0.009 ± 0.004	0.007 ± 0.0055	
	L	1.39 ± 1.08	1.17 ± 0.73		0.15 ± 0.19	0.076 ± 0.124		0.011 ± 0.009	0.01 ± 0.007	
Temporal lobe	R	1.5 ± 0.57*	0.9 ± 0.72	−40	0.014 ± 0.032	0.024 ± 0.048		0.0065 ± 0.002*	0.0038 ± 0.0028	−42
	L	1.48 ± 0.28*	0.61 ± 0.43	−58	0.33 ± 0.20*	0.069 ± 0.09	−79	0.0076 ± 0.0025*	0.0035 ± 0.003	−54
Occipital lobe	R	1.14 ± 0.66	0.97 ± 0.95		0.02 ± 0.046	0.12 ± 0.32		0.005 ± 0.0028	0.006 ± 0.0068	
	L	0.93 ± 0.77	0.8 ± 0.80		0.019 ± 0.025	0.102 ± 0.17		0.0083 ± 0.0064	0.0061 ± 0.004	
Insula	R	1.72 ± 0.79*	0.95 ± 0.87	−45	0.42 ± 0.3	0.19 ± 0.27		0.0084 ± 0.0028	0.0052 ± 0.004	
	L	1.25 ± 0.55	1.11 ± 0.79		0.099 ± 0.1	0.054 ± 0.06		0.0081 ± 0.0068	0.0086 ± 0.0079	
Amygdala	R	1.44 ± 0.39*	0.66 ± 0.62	−54	0.079 ± 0.078	0.023 ± 0.035		0.0064 ± 0.0028*	0.0033 ± 0.0028	−48
	L	1.59 ± 0.53*	0.65 ± 0.63	−59	0.072 ± 0.1*	0.0019 ± 0.007	−97	0.0075 ± 0.0029*	0.0029 ± 0.0019	−61
Thalamus	R	1.21 ± 0.26*	0.73 ± 0.59	−40	0.087 ± 0.089	0.049 ± 0.076		0.0099 ± 0.0067	0.0046 ± 0.0039	
	L	0.7 ± 0.24	0.64 ± 0.58		0.135 ± 0.06*	0.049 ± 0.055	−64	0.0213 ± 0.030	0.0077 ± 0.0076	
Caudate	R	1.85 ± 0.27*	1.12 ± 0.83	−39	0.049 ± 0.10	0.04 ± 0.092		0.0121 ± 0.0084	0.0258 ± 0.0214	
	L	2.36 ± 0.73*	1.41 ± 0.87	−40	0.022 ± 0.05	0.031 ± 0.093		0.0160 ± 0.0044*	0.0097 ± 0.0087	−39
Putamen	R	1.81 ± 0.35*	1.13 ± 0.71	−38	0.10 ± 0.16	0.14 ± 0.21		0.0108 ± 0.0031	0.0072 ± 0.005	
	L	1.48 ± 0.26	1.13 ± 0.63		0.022 ± 0.035	0.108 ± 0.27		0.0086 ± 0.003	0.0072 ± 0.004	
Hypothalamus	R	1.2 ± 0.35	0.79 ± 0.78		0.099 ± 0.14	0.101 ± 0.15		0.0089 ± 0.0035	0.0066 ± 0.0069	
	L	1.13 ± 0.27*	0.41 ± 0.30	−64	0.097 ± 0.075	0.091 ± 0.09		0.0101 ± 0.0055*	0.0035 ± 0.0030	−65
Pituitary	–	2.05 ± 0.46	2.0 ± 0.89		0.22 ± 0.28	0.08 ± 0.11		0.0121 ± 0.0025	0.0137 ± 0.007	
Cerebellum	R	1.11 ± 0.88	1.22 ± 0.73		0.045 ± 0.056	0.26 ± 0.57		0.008 ± 0.006	0.0199 ± 0.024	
	L	1.63 ± 0.72	1.42 ± 1.00		0.08 ± 0.166	0.036 ± 0.067		0.013 ± 0.0085	0.0079 ± 0.0055	
Mesencephalon	R	0.64 ± 0.51	0.58 ± 0.54		0.23 ± 0.13	0.14 ± 0.11		0.008 ± 0.007	0.006 ± 0.005	
	L	1.14 ± 0.93	0.52 ± 0.47		0.117 ± 0.11*	0.032 ± 0.052	−73	0.0097 ± 0.008	0.0043 ± 0.0038	
Protuberance	R	2.33 ± 0.50*	1.12 ± 1.03	−52	0.128 ± 0.28	0.033 ± 0.073		0.014 ± 0.0055	0.0077 ± 0.0066	
	L	2.1 ± 0.39*	1.09 ± 1.01	−48	0.194 ± 0.18	0.185 ± 0.37		0.0173 ± 0.007*	0.0078 ± 0.0077	−55
Medulla oblongata	R	1.12 ± 0.43*	0.35 ± 0.37	−69	0.156 ± 0.17	0.085 ± 0.13		0.0056 ± 0.004*	0.0018 ± 0.0017	−68
	L	1.22 ± 0.57*	0.47 ± 0.43	−61	0.17 ± 0.17	0.095 ± 0.089		0.0066 ± 0.0047*	0.0018 ± 0.0014	−72
Spinal cord	D	0.42 ± 0.17	0.38 ± 0.35		0.053 ± 0.052	0.059 ± 0.05		0.0018 ± 0.0006	0.003 ± 0.003	
	V	0.72 ± 0.44*	0.26 ± 0.23	−63	0.196 ± 0.09*	0.104 ± 0.058	−47	0.005 ± 0.0022*	0.0021 ± 0.0018	−58
Bichat fat pad	–	0.033 ± 0.009	0.033 ± 0.009		0.136 ± 0.056	0.1 ± 0.044		0.0004 ± 0.0002	0.0005 ± 0.0003	
SC abdominal fat	–	0.036 ± 0.036	0.017 ± 0.007		0.095 ± 0.041*	0.073 ± 0.041	−23	0.0023 ± 0.002	0.0036 ± 0.0033	
SC lower limbs fat	–	0.029 ± 0.007	0.03 ± 0.015		0.167 ± 0.053	0.124 ± 0.049		0.0017 ± 0.0006*	0.0011 ± 0.0006	−35
Visceral fat	–	0.03 ± 0.01*	0.020 ± 0.01	−33	0.130 ± 0.086*	0.056 ± 0.039	−57	0.0013 ± 0.0009	0.0017 ± 0.001	

(*continued on next page*)

Table 5 (*continued*)

Tissues	Side	*BSCL2*-203			*BSCL2*-205/207/210			*BSCL2*-201		
		< 61 y. (n = 6)	≥61 y. (n = 7)	Δ%	< 61 y. (n = 6)	≥61 y. (n = 7)	Δ%	< 61 y. (n = 6)	≥61 y. (n = 7)	Δ%
Rectus abdominis muscle	–	0.05 ± 0.01	0.050 ± 0.016		0.103 ± 0.043	0.141 ± 0.09		0.0018 ± 0.0008	0.0014 ± 0.0007	
Gastrocnemius muscle	–	0.032 ± 0.015	0.036 ± 0.018		0.036 ± 0.027	0.058 ± 0.056		0.0032 ± 0.0055	0.0066 ± 0.011	
Myocardium	–	0.018 ± 0.0075	0.0126 ± 0.0045		0.038 ± 0.009*	0.033 ± 0.02	−13	0.00054 ± 0.0001*	0.0003 ± 0.0002	−44
Liver	–	0.025 ± 0.006*	0.0149 ± 0.008	−40	0.045 ± 0.017	0.033 ± 0.025		0.0005 ± 0.00036	0.00048 ± 0.0003	
Vagus nerve	–	0.116 ± 0.024*	0.059 ± 0.017	−49	0.107 ± 0.043	0.080 ± 0.036		0.00065 ± 0.0003	0.00045 ± 0.0002	
Trigeminal nerve	–	0.296 ± 0.177	0.191 ± 0.089		0.142 ± 0.105	0.108 ± 0.09		0.0026 ± 0.0018*	0.0012 ± 0.0012	−54
Renal cortex	–	0.08 ± 0.019	0.07 ± 0.025		0.162 ± 0.077	0.56 ± 1.05		0.002 ± 0.001	0.00266 ± 0.0023	
Renal medulla	–	0.093 ± 0.042	0.091 ± 0.059		0.166 ± 0.104*	0.61 ± 0.62	267	0.0037 ± 0.0025	0.0067 ± 0.006	
Gonads	–	0.466 ± 0.211	0.393 ± 0.599		1.048 ± 0.49*	0.31 ± 0.58	−70	0.0075 ± 0.0035*	0.0041 ± 0.0046	−45

Relative expression of the encephalic and non-encephalic post-mortem tissues in young and old subjects, *: $p < 0.05$. All samples were analyzed in duplicate, n = 13. Results were normalized for the *18S* gene.

PNS, and 12.4% in ET (Fig. 3B), and the pituitary and the gonads had the highest total *BSCL2* expression of the non-neural tissues (5.25% and 2.61%, respectively). The predominant transcript is *BSCL2*-203 (×6.8), which encodes the long isoform and represents 86.6% of total *BSCL2* transcript expression (Fig. 3B). *BSCL2*-203 was expressed most in the CNS (78.9% of total *BSCL2* expression, and 91.2% of *BSCL2*-203 expression) (Fig. 3B, C) and was higher in the caudate nuclei and in the protuberance (9.2% and 9% of *BSCL2*-203 expression, respectively). *BSCL2*-203 expression in the PNS and ET was 0.9% and 7.9%, respectively (Fig. 3C). *BSCL2*-205/207/210 expression represented only 12.7% of total *BSCL2* expression (Fig. 3B) and was expressed the most in ET and the PNS (42.6% and 4.1% of *BSCL2*-205/207/210 expression, respectively) (Fig. 3C). *BSCL2*-205/207/210 expression was increased 3.9× and 2× respectively in adipose and muscle tissues, compared to *BSCL2*-203, and *BSCL2*-201 expression was low in all tissues (0.7% of total *BSCL2* expression, Fig. 3B). Within the CNS, the short transcript was primarily expressed in the caudate nucleus, the cerebellum, and the protuberance. Expression levels of *BSCL2* transcripts across the primary brain divisions are summarized in Fig. 3C.

A comparison of *BSCL2* expression between men and women (Table 4) shows that the three transcripts are expressed more highly in the testicles than in the ovaries (*BSCL2*-203: +54%, $p = 0.003$; *BSCL2*-205/207/210: +2559%, $p = 0.0001$; *BSCL2*-201: +345%, $p = 0.0001$), and *BSCL2*-203 and *BSCL2*-205/207/210 are more expressed in the ventral spinal cord in men than in women (+164%, $p = 0.008$; and +71%, $p = 0.02$, respectively). *BSCL2*-203 expression is significantly higher in the temporal lobe in men than in women (Right: +57%, $p = 0.046$; Left: +46%, $p = 0.04$), the visceral fat (–33%, $p = 0.023$), and the vagus nerve (+43%, $p = 0.017$) (Table 4). *BSCL2*-205/207/210 expression in the left temporal lobe (+408%, $p = 0.01$), left insula (+194%, $p = 0.01$), left hypothalamus (+155%, $p = 0.01$), subcutaneous abdominal fat (+69%, $p = 0.003$), and vagus and trigeminal nerves (+83%, $p = 0.001$; and +108%, $p = 0.018$, respectively) are significantly higher in men than in women, while expression in men is lower in the rectus abdominis muscle and the left frontal lobe (−42%, $p = 0.015$; −63%, $p = 0.02$, respectively) (Table 4) compared to women. Finally, *BSCL2*-201 expression in the pituitary and the right cerebellum are significantly lower in men than in women (−40%, $p = 0.003$, and −67%, $p = 0.015$, respectively) (Table 4).

Influence of age on *BSCL2* expression

A comparison of *BSCL2* expression between young and aged individuals (median age 61 years, Table 5) shows that *BSCL2* transcripts are generally expressed more highly in younger subjects in both encephalic and non-encephalic tissues. This observation is strongest for *BSCL2*-203 (Table 5), weaker for *BSCL2*-201, and weakest for *BSCL2*-205/207/210. An analysis of the correlations between *BSCL2*-203 transcript and age

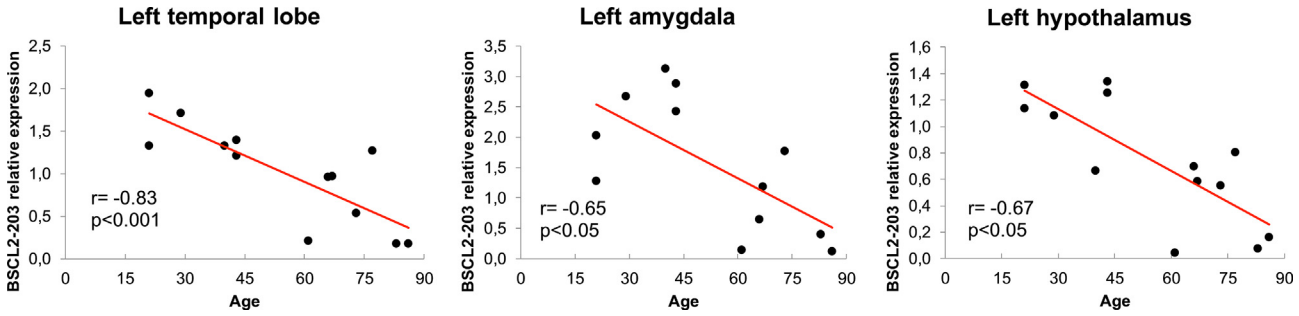

Fig. 4. Correlations between *BSCL2* and age. Spearman's correlation was calculated between *BSCL2*-203 relative expression normalized to the *18S* gene and age. Significant correlations were observed for each zone: left temporal lobe, left amygdala and left hypothalamus, $n = 13$.

using Spearman's correlation coefficient revealed significant negative correlations in the left temporal lobe ($r = -0.83$, $p < 0.001$), left hypothalamus ($r = -0.67$, $p < 0.05$), and left amygdala ($r = -0.62$, $p < 0.05$) (Fig. 4).

Putative role for seipin on oxidative stress protection and peroxisome biogenesis in the CNS

qPCR studies in human brains. Based on the previous correlation results, the well-known role for oxidative stress in aging (López-Otín et al., 2013), and our own preadipocyte proteomic results from Celia's Encephalopathy case (Ruiz-Riquelme et al 2015) indicating that mitochondrial superoxide dismutase (*SOD2*) and glutathione peroxidase were distinctively modulated, we decided to quantify the expression of key genes related to oxidative stress protection by qPCR in the left temporal lobe, left amygdala and left hypothalamus: *PPARG*, cytoplasmic superoxide dismutase (*SOD1*), mitochondrial superoxide dismutase (*SOD2*), catalase (*CAT*), peroxisomal biogenesis factor 1 (*PEX1*), peroxisomal biogenesis factor 11 gamma (*PEX11G*) and peroxisomal biogenesis factor 16 (*PEX16*). Spearman's correlation coefficients were calculated and strong positive correlations were found between *BSCL2*-203 and *SOD1* and *SOD2*: *BSCL2*-203/*SOD1*, $r = 0.85$, $p < 0.001$ and *BSCL2*-203/*SOD2*, $r = 0.88$, $p < 0.001$, in left amygdala; *BSCL2*-203/*SOD1*, $r = 0.79$, $p < 0.05$ and *BSCL2*-203/*SOD2*, $r = 0.82$, $p < 0.05$, in left temporal lobe; *BSCL2*-203/*SOD1*, $r = 0.95$, $p < 0.001$ and *BSCL2*-203/*SOD2*, $r = 0.82$, $p < 0.05$, in the left hypothalamus. We found an important positive correlation between *PPARG* and *BSCL2*-203 in the amygdala and hypothalamus ($r = 0.93$, $p < 0.001$, in left amygdala; $r = 0.9$, $p < 0.001$, in left hypothalamus). Considering that PPARG plays an important role in the activation of peroxisome proliferation, we measured the expression of *PEX1*, *PEX11G*, and *PEX16*. *PEX1* encodes peroxisome biogenesis factor 1, an ATP-ase anchored to the peroxisomal membrane, and plays a role in protein import into peroxisomes and peroxisome biogenesis. *PEX11G*, member of the PEX11 family proteins, is involved in peroxisome fission, while *PEX16*, a *PPARG* target gene, is required for *de novo* synthesis of peroxisomes. *BSCL2* did not correlate with *PEX1* when applying partial correlation coefficients, but positive correlations were found between *BSCL2*-203 and *PEX11G*: $r = 0.67$, $p < 0.05$ in left hypothalamus, $r = 0.65$, $p < 0.05$ in left temporal lobe, and $r = 0.62$, $p < 0.05$ in left amygdala; and also between *BSCL2*-203 and *PEX16* in left amygdala: $r = 0.81$, $p < 0.05$. The catalase enzyme (*CAT*), present in peroxisomes, correlated with *BSCL2*-203 in left hypothalamus: $r = 0.82$, $p < 0.05$, in left temporal lobe: $r = 0.91$, $p < 0.05$, and in left amygdala, $r = 0.63$, $p < 0.05$ (Fig. 5).

In vitro studies. Since the observed correlations do not imply causality, we differentiate SH-SY5Y cells stably transfected with *BSCL2* into a neuronal model cell line in order to measure the expression of genes significantly correlated with *BSCL2* in human brains. Morphological changes were observed after 3–5 days (Fig. 6), and many SH-SY5Y cells stopped proliferating and expanded an extensive network of long neurites. At the end of differentiation (day 7), cells were evenly distributed and developed a more rounded shape, forming clumps of cell bodies linked by long processes similar to axons (Fig. 6C).

Neuronal differentiation was assessed by quantifying the mRNA expression levels of neurogenesis-related genes specific for neural progenitors (*NESTIN*) and mature neurons (*NeuN/RBFOX3*), playing an essential role in the differentiation and maturation of neural progenitor cells (Kim et al., 2009; Kim et al., 2013). The results showed that the mRNA expression of both neuronal markers was detected in non-differentiated cells and significantly increased after 7 days of differentiation, pointing toward a more neuronal phenotype. *NESTIN* and *NeuN/RBFOX3* increased approximately 4- to 5-fold and 2- to 10-fold, respectively, (Fig. 7A, B). The expression of the *BSCL2*-203 transcript was much higher in *BSCL2*-cells than in control cells (+3024%) (Fig. 8A). While there was no significant difference for *PEX1*, significantly higher relative expression was seen for *PEX11G* (+491%) (Fig. 8H), *PEX16* (+181%) (Fig. 8G), *PPARG* (+93%) (Fig. 8C), the antioxidant enzymes *SOD1* (+33%) (Fig. 8D), *SOD2* (+25%) (Fig. 8E), and *CAT* (+58%) (Fig. 8F).

Confocal microscopy studies in human brains. Confocal microscopy was used to localize seipin and PEX16 expression in the hypothalami of healthy human brains

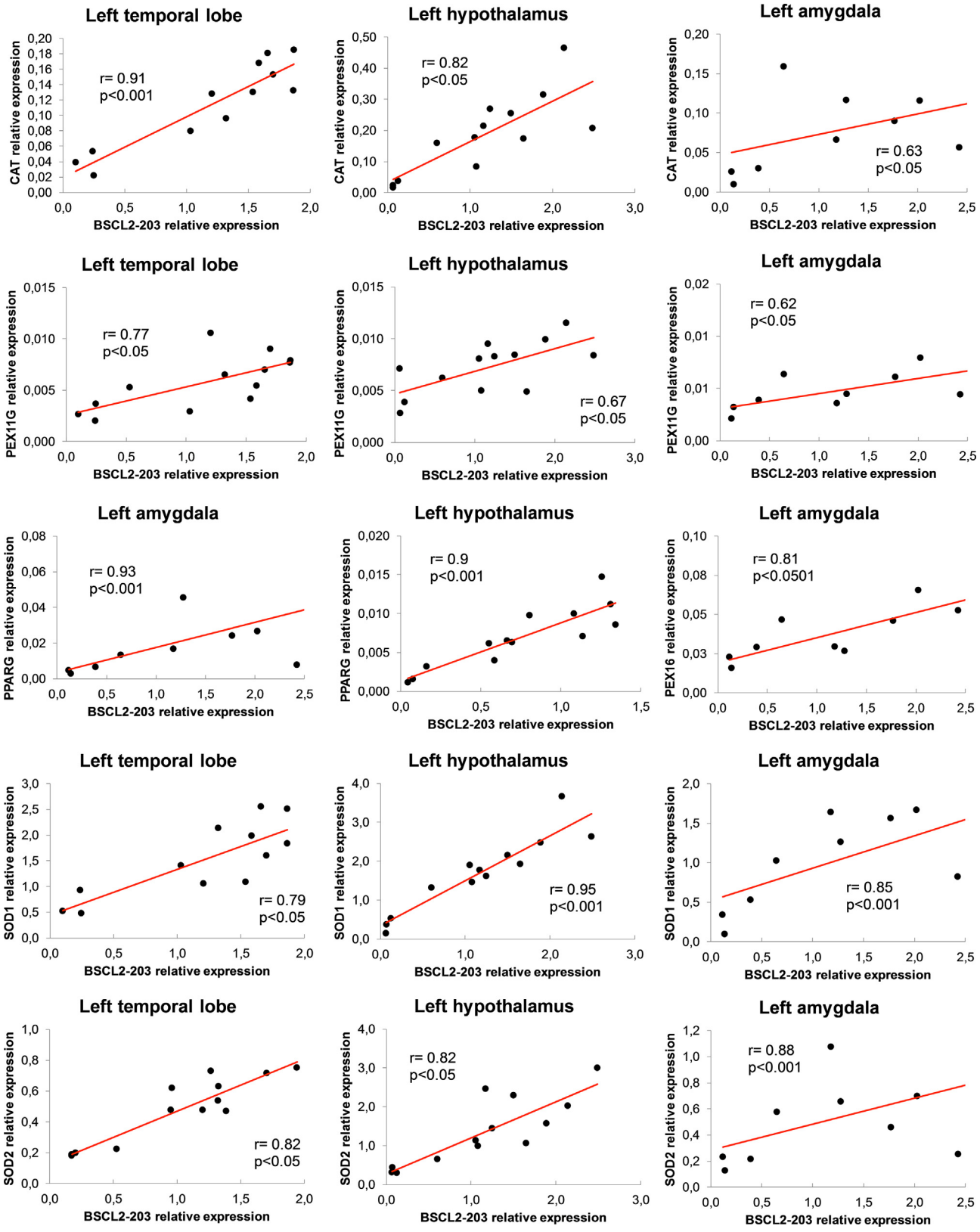

Fig. 5. Correlations between *BSCL2* and other genes. Spearman's correlations were calculated for *BSCL2*-203, *CAT*, *PEX11G*, *PEX16*, *PPARG*, *SOD1 and SOD2* relative expressions, normalized to the *RPII* gene. Significant correlations were observed in the following zones: left temporal lobe, left amygdala and left hypothalamus, $n = 13$.

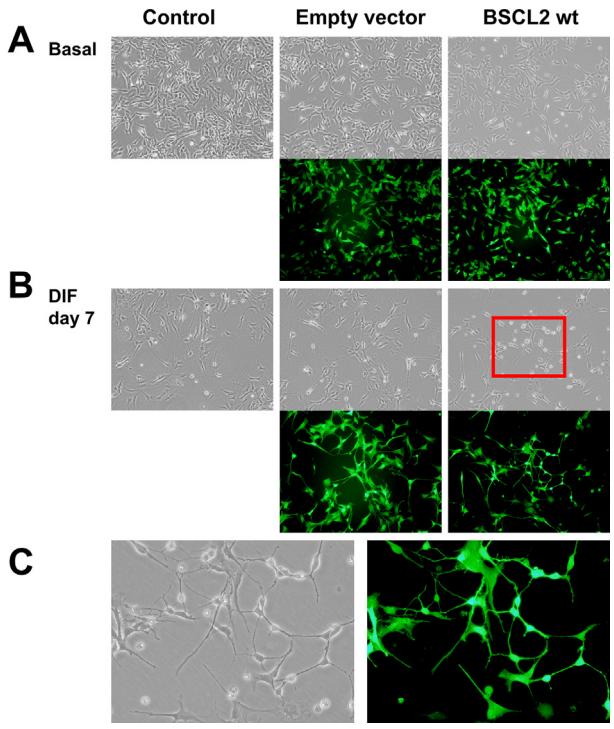

Fig. 6. Morphological comparison between undifferentiated and differentiated SH-SY5Y, Morphological comparison between (A) undifferentiated and (B) differentiated SH-SY5Y cells over 7 days. Phase contrast light microscopy and GFP fluorescence images visualized under 10× magnification. Small red box indicates zoomed area (C), shown under 20× magnification.

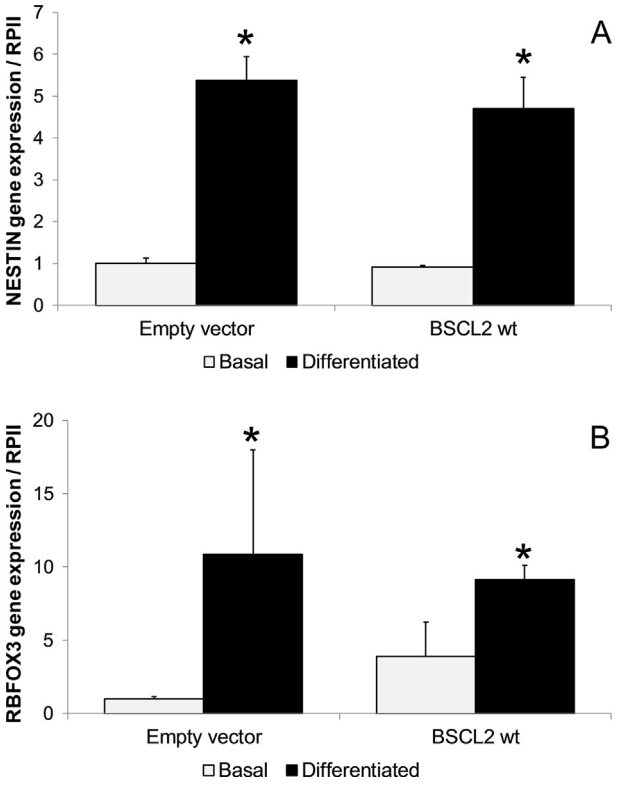

Fig. 7. Variation of neuronal markers after differentiation. Relative expression of neuronal markers: (A) *NESTIN* and (B) *NeuN/RBFOX3*, $^{*}p < 0.05$ vs basal. All samples were analyzed in duplicate, $n = 4$. Results were normalized to the *RNA polymerase II* gene.

and the PELD case. Image analysis revealed that seipin and PEX16 are expressed in neurons in the hypothalamic nuclei of both controls but not the PELD index case (Fig. 9A–C). Interestingly, we only found cytoplasmic seipin in neurons (and not in astrocytes or oligodendrocytes). The main pattern observed in control brain regions was what we classified as the "granular profile," in which seipin is scattered throughout the neuronal cytoplasm and PEX16 appears to be closely intertwined in the free spaces (Fig. 9A, B) very close to seipin, with a shape resembling vesicles (Fig. 9D). We also observed intranuclear PEX16 and seipin in control hypothalamus images (Fig. 9B). Finally, the seipin observed in neurons was localized in the cytoplasm in samples from Celia's Encephalopathy case, and the staining was clearly diffused within the neuronal body and the proximal segment of the axons. There were more seipin-containing nuclei in Celia's Encephalopathy case compared to the control, while no PEX16 was found in the hypothalamus of this patient (Fig. 9C).

DISCUSSION

This study describes the differential expression of the *BSCL2* in the human brain and other tissues, and identifies *BSCL2*-203 as the major transcript in the CNS. Remarkably, expression of this transcript appears to be reduced in the more primitive regions of the brain (diencephalon, mesencephalon and rhombencephalon). *BSCL2-205/207/210* is primarily expressed in the extraneural tissues, and the transcript responsible for the Celia-seipin (*BSCL2*-201) is expressed very little but mainly in the caudate, one of the nuclei affected earliest in Celia's Encephalopathy (Araujo-Vilar et al., 2018). These results indicate specific tissue functions for the different *BSCL2* transcripts, and these results coupled with the observation that the 64 amino acids corresponding to exon 1 and part of exon 2 of the *BSCL2*-203 transcript are identical or quasi-identical in hominidae primates (100–98%), very similar in other catarrhine primates (95%), and similar in platyrrhine primates (86–89%), while similarities are reduced in prosimians (75–55%) and in mice (52%) (Fig. 10) suggest that the longer transcript should play some role in the encephalization process.

To the best of our knowledge, this is the first time that *BSCL2* transcript expression is mapped in the different regions of human brain. In mice, Garfield et al. (2012) using *in situ* hybridization to map the location of Bscl2 mRNA-positive cells, found that the regions with strong expression were the basal forebrain, hippocampus, hypothalamus, dorsal and ventral brainstems, with low expression in the cortex, moderate expression in the midbrain and no detectable expression in the caudate putamen. On the other hand, Liu et al. (2016) found a similar expression pattern of seipin in the CNS using immuno-histochemical staining, however with some discrepancies like in the caudate putamen. While in our study, we found highest *BSCL2* expression in caudate, putamen, cerebellum and protuberance, and mostly in

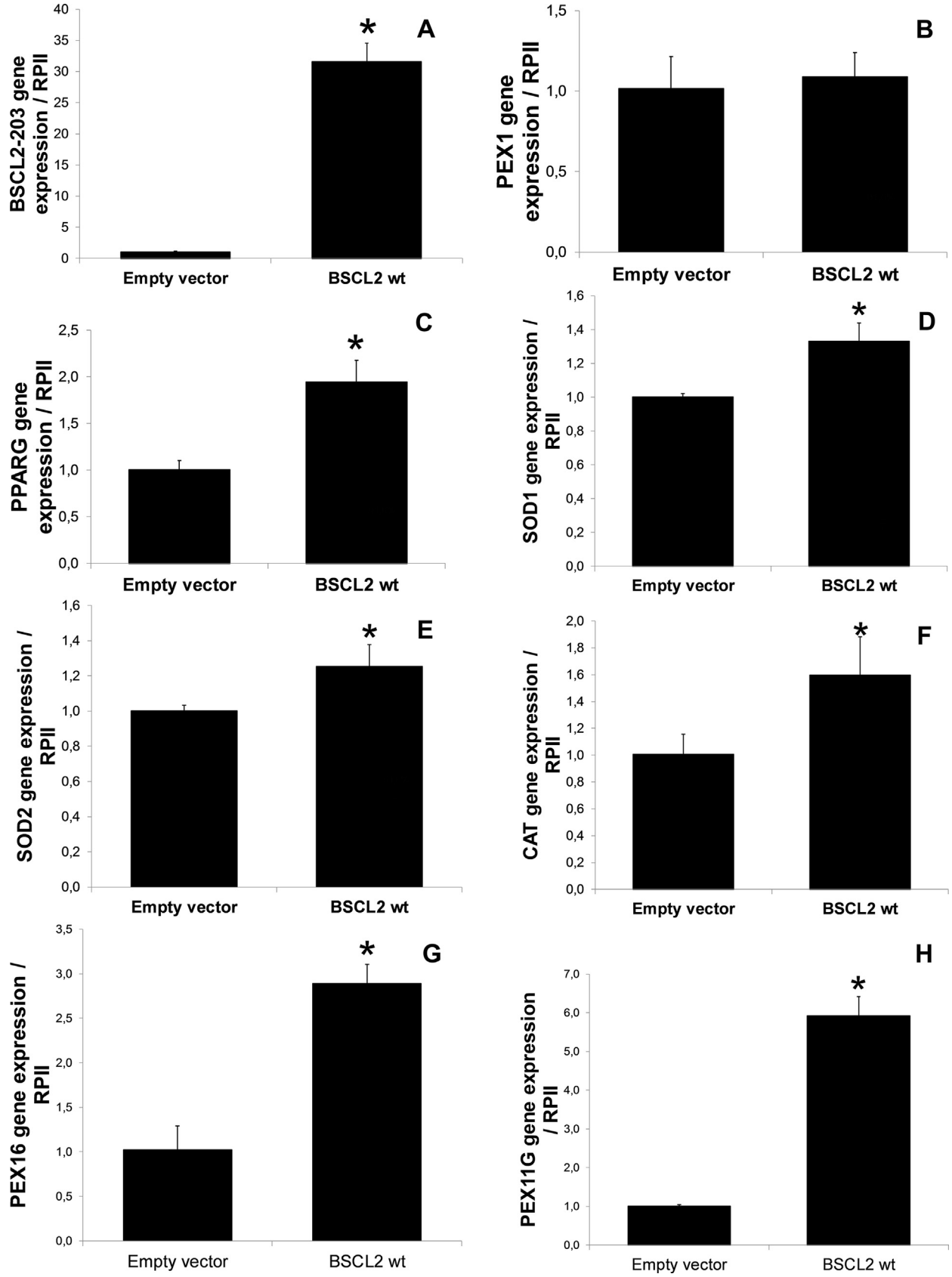

Fig. 8. Relative gene expression in SH-SY5Y differentiated cells overexpressing *BSCL2*-203 transcript. Relative expression of: (A) *BSCL2*-203, (B) *PEX1*, (C) *PPARG*, (D) *SOD1*, (E) *SOD2*, (F) *CAT*, (G) *PEX11G*, (H) *PEX16*, $^{*}p < 0.05$ vs cells transfected with empty vector. All samples were analyzed in duplicate, $n = 4$. Results were normalized to the *RNA polymerase II* gene.

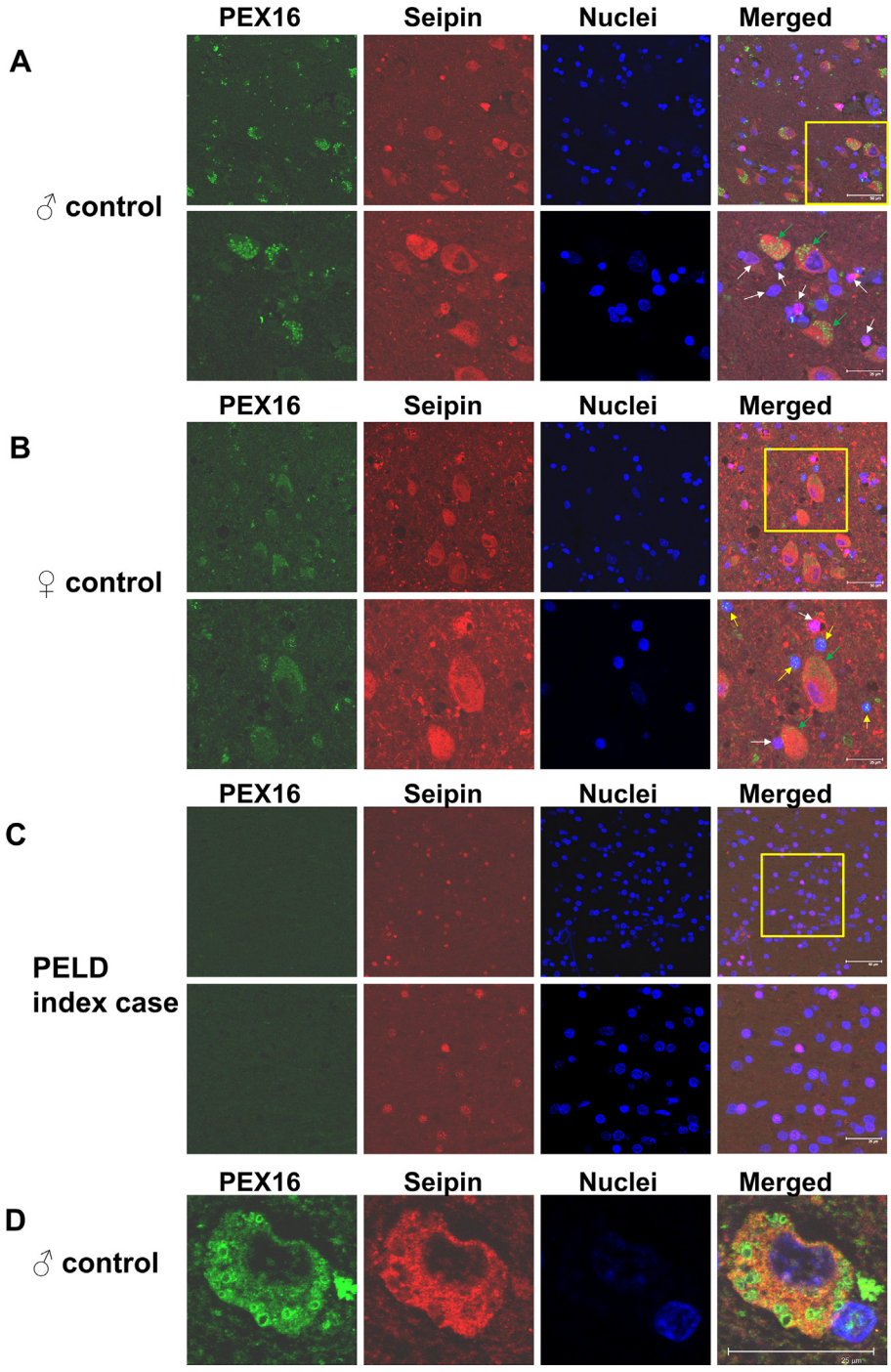

Fig. 9. Confocal microscopy images. Confocal microscopy images (under 63 × magnification with 2×-zoomed images also included) showing immunofluorescence staining in the hypothalamus (HT) of (A) one male control case (59-year-old), (B) one female control case (75-year-old), and (C) the PELD index case, for PEX16 (green, Alexa 488), seipin (red, Alexa 555), and DAPI to label nuclei. Maximum image projection shows the granular profile (green arrow), intranuclear seipin (white arrow), and intranuclear PEX16 (yellow arrow), and merged images show no overlap between PEX16 and seipin (B). Analysis of the view from one section from the male control case indicates that PEX16 labeling was located as a peripheral ring, suggesting membrane labeling of vesicle-like PEX16 (D). Scale bar 25 and 50 μm. (For interpretation of the references to color in this figure legend, the reader is referred to the web version of this article.)

the forebrain and hindbrain. Inter-species differences could explain these discrepancies.

We have also found that the expression of seipin is noticeably reduced in the temporal lobe, amygdala and hypothalamus of the left hemisphere with age, all areas associated with memory and its consolidation, and the limbic system. Given that mitochondrial dysfunction is one of the hallmarks of aging (López-Otín et al., 2013), and that the proteomic results in preadipocytes of Celia's Encephalopathy index case (Ruiz-Riquelme et al., 2015b) indicated that mitochondrial superoxide dismutase (SOD2) and glutathione peroxidase were distinctively modulated, it is not surprising to find strong positive correlations between *BSCL2* and protective enzymes against oxidative stress such as *CAT*, *SOD1* and *SOD2*. The positive correlations between *BSCL2* and *PPARG*, in agreement with other studies (Li et al., 2015; Qian et al., 2016; Zhou et al., 2016), *CAT*, *SOD1*, or *SOD2* could be explained by the important role played by *PPARG* in the activation of peroxisome proliferation, ultimately protecting against neurodegeneration by reducing the production of reactive oxygen species (Nordgren and Fransen, 2014; Cipolla and Lodhi 2017). On the other hand, peroxisomal proliferation also reduces beta-amyloid-induced toxicity in hippocampal neurons, reducing neuronal death and the loss of the neuritic network (Santos et al., 2005).

We investigated whether seipin is truly related to protective enzymes and peroxisomes in order to confirm our qPCR results in human brains. The significantly increased expression of the *PEX11G*, *PEX16*, *SOD1*, *SOD2*, *CAT*, and *PPARG* genes corroborated the relationship between seipin and the protective proteins to oxidative stress in differentiated SH-SY5Y cells overexpressing *BSCL2*. Confocal microscopy in the hypothalami of healthy human brains also confirmed the close juxtaposition of seipin and *PEX16*, the latter appearing with a vesicle-like shape. This key protein for peroxisomal biogenesis is required for the de novo synthesis of peroxisomes (Kim et al., 2006) and is known to target to the ER before being trafficked to peroxisomes (Hua et al., 2015). Hofer et al.

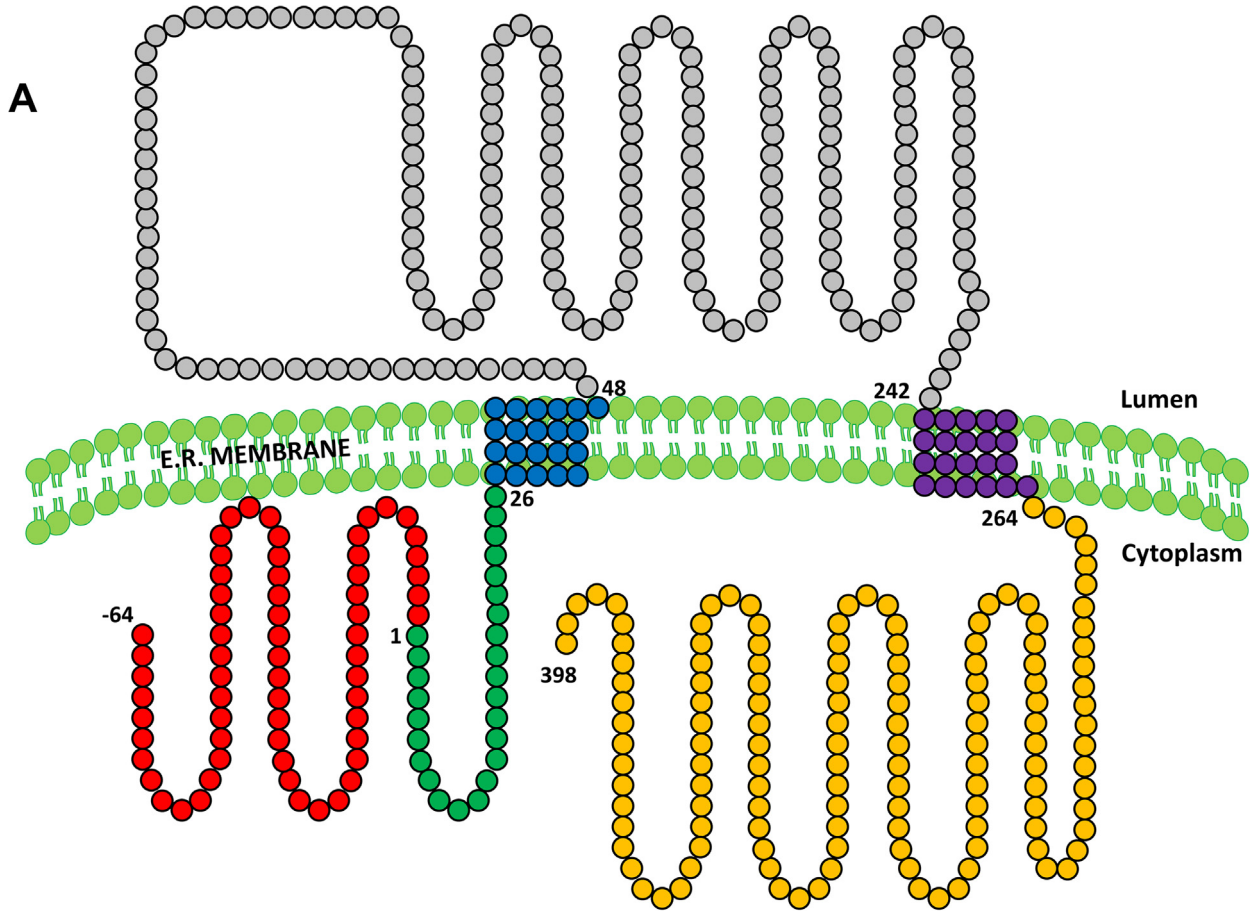

Fig. 10. Seipin topology and homology. (A) The 462-residue-long form of seipin has two transmembrane helices, the N- and C-cytosolic-termini appear to be variable among species, but the central domain loop at the lumen of the ER is highly conserved (B). CYT: cytoplasmic, TMD: transmembrane, LUM: lumenal.

recently showed that *PEX16* is a *PPAR*G target gene whose expression regulates peroxisome number and lipid metabolism, and demonstrated that it is also required for adipogenesis (Hofer et al., 2017). Studies in rodents have shown the beneficial effects of the pharmacological activation of peroxisome proliferator-activated receptors in Parkinson's disease and dyskinesia models (Barbiero et al., 2014; Grover et al., 2013).

The profiles observed in the confocal images suggest that seipin is involved in peroxisome biogenesis, probably at an early phase. The juxtaposition of seipin and *PEX16* observed in some neurons is consistent with the potential close proximity of peroxisomes and lipid droplet biogenesis areas (Binns et al., 2006), suggesting that peroxisomes and seipin are intimately associated. We can further speculate that peroxisomes with vesicle-like shapes may be pre-peroxisomal vesicles emerging from the ER. It should be noted that the structure of the lipid droplets and the peroxisomes are similar, both emerge from the ER, and there is a dialog between both organelles (Shai et al., 2016). In this line, very recently and during the course of the review of this manuscript, Wang et al. 2018 identify in yeasts Pex30 as a factor cooperating with seipin in the biogenesis of both lipid droplets and pre-peroxisomal vesicles from the ER. In our opinion, this recent Wang's paper reinforces our hypothesis about the role of seipin in peroxisomes biogenesis. On the other hand, peroxisomes are very abundant in neurons and play a key role in protection against oxidative stress, and are also critical for the synthesis of phospholipids. Finally, the peroxisome biomarker *PEX16* is barely detectable in the brain of the PELD case, where seipin is also scarce. Taken together, these data may suggest that seipin is playing a role in peroxisome biogenesis as a regulator of peroxisomal protein sorting during the first steps of biogenesis from the ER, similarly to what happens in the nascent lipid droplets (Shai et al., 2016; Wang et al. 2018), or could act as an essential factor in the recruitment of other peroxisomal membrane proteins to the ER together with *PEX16,* which subsequently transports them to the peroxisomes (Kim and Mullen, 2013). Correlation studies of gene expression, lentiviral overexpression experiments, as well as immunohistochemical and localization studies have allowed us to consolidate our hypotheses regarding the pathogenetic mechanisms of Celia's Encephalopathy (Ruiz-Riquelme et al., 2015). Seipin appears to have specific functions in the CNS, and could act as a neuroprotector, modulating the expression of *SOD* and *CAT* via *PPARG* by unknown mechanisms and promoting the proliferation of peroxisomes,

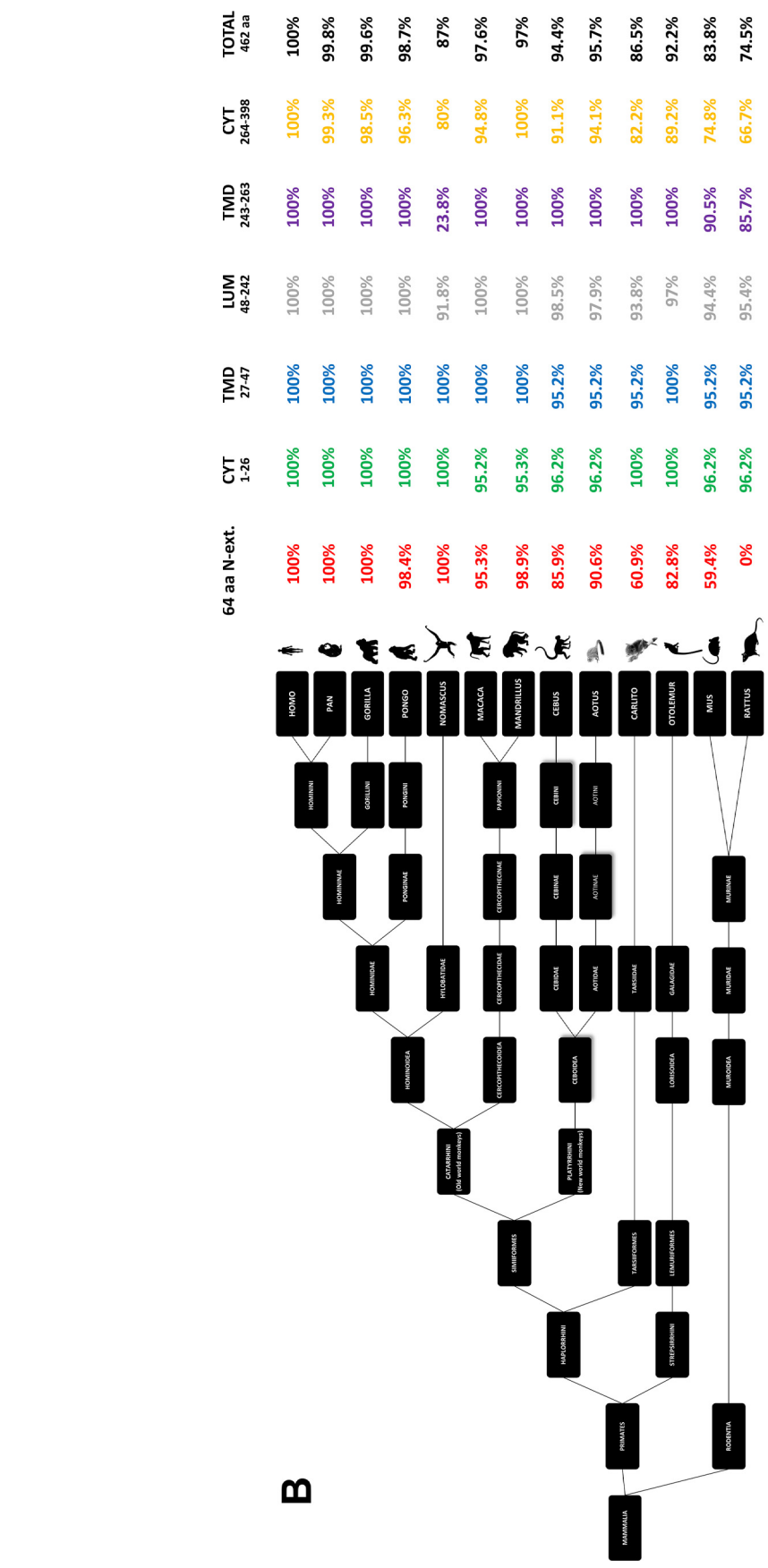

Fig. 10 (*continued*)

thus decreasing free radicals and consequently protecting against neurodegeneration. The fact that seipin may be playing a role in peroxisome biogenesis makes them an interesting potential therapeutic target.

ACKNOWLEDGMENTS

We are indebted to the parents of the patient for their collaboration in this study. We acknowledge confocal technical assistance by Mercedes Rivas Cascallar.

This work was supported by the Instituto de Salud Carlos III and the European Regional Development Fund, FEDER (grants number PI10/02873 and PI13/00314), by the Consellería de Industria, Xunta de Galicia (grants number 10PXIB208013PR and ED341b 2017/19), and by Fundación Mutua Madrileña (Call 2015).

COMPETING INTERESTS

The authors have no conflicts of interest to declare.

REFERENCES

Alaei MR, Talebi S, Ghofrani M, Taghizadeh M, Keramatipour M (2016) Whole exome sequencing reveals a BSCL2 mutation causing progressive encephalopathy with lipodystrophy (PELD) in an Iranian pediatric patient. Iran Biomed J 20:295–301.

Araujo-Vilar D, Domingo-Jiménez R, Ruibal Á, Aguiar P, Ibáñez-Micó S, Garrido-Pumar M, Martínez-Olmos MÁ, López-Soler C, Guillín-Amarelle C, González-Rodríguez M, et al. (2018) Association of metreleptin treatment and dietary intervention with neurological outcomes in Celia's encephalopathy. Eur J Hum Genet 26:396–406. https://doi.org/10.1038/s41431-017-0052-8.

Barbiero JK, Santiago RM, Persike DS, da Silva Fernandes MJ, Tonin FS, da Cunha C, Lucio Boschen S, Lima MM, Vital MA (2014) Neuroprotective effects of peroxisome proliferator-activated receptor alpha and gamma agonists in model of parkinsonism induced by intranigral 1-methyl-4-phenyl-1,2,3,6-tetrahyropyridine. Behav Brain Res 274:390–399. https://doi.org/10.1016/j.bbr.2014.08.014.

Binns D, Januszewski T, Chen Y, Hill J, Markin VS, Zhao Y, Gilpin C, Chapman KD, Anderson RG, Goodman JM (2006) An intimate collaboration between peroxisomes and lipid bodies. J Cell Biol 173:719–731. https://doi.org/10.1083/jcb.200511125.

Cartwright BR, Goodman JM (2012) Seipin: from human disease to molecular mechanism. J Lipid Res 53:1042–1055. https://doi.org/10.1194/jlr.R023754.

Cipolla CM, Lodhi IJ (2017) Peroxisomal dysfunction in age-related diseases. Trends Endocrinol Metab 28:297–308. https://doi.org/10.1016/j.tem.2016.12.003.

Ebihara C, Ebihara K, Aizawa-Abe M, Mashimo T, Tomita T, Zhao M, Gumbilai V, Kusakabe T, Yamamoto Y, Aotani D (2015) Seipin is necessary for normal brain development and spermatogenesis in addition to adipogenesis. Hum Mol Genet 24:4238–4249. https://doi.org/10.1093/hmg/ddv156.

Garfield AS, Chan WS, Dennis RJ, Ito D, Heisler LK, Rochford JJ (2012) Neuroanatomical characterisation of the expression of the lipodystrophy and motor-neuropathy gene Bscl2 in adult mouse brain. PLoS One 7(9). https://doi.org/10.1371/journal.pone.0045790 e45790.

Grover S, Kumar P, Singh K, Vikram V, Budhiraja RD (2013) Possible beneficial effect of peroxisome proliferator-activated receptor (PPAR)-alpha and gamma agonist against a rat model of oral dyskinesia. Pharmacol Biochem Behav 111:17–23. https://doi.org/10.1016/j.pbb.2013.08.001.

Guillen-Navarro E, Sánchez-Iglesias S, Domingo-Jiménez R, Victoria B, Ruiz-Riquelme A, Rábano A, Loidi L, Beiras A, González-Méndez B, Ramos A, et al. (2013) A new seipin-associated neurodegenerative syndrome. J Med Genet 50:401–409. https://doi.org/10.1136/jmedgenet-2013-101525.

Hofer DC, Pessentheiner AR, Pelzmann HJ, Schlager S, Madreiter-Sokolowski CT, Kolb D, Eichmann TO, Rechberger G, Bilban M, Graier WF, et al. (2017) Critical role of the peroxisomal protein PEX16 in white adipocyte development and lipid homeostasis. Biochim Biophys Acta Mol Cell Biol Lipids 1862:358–368. https://doi.org/10.1016/j.bbalip.2016.12.009.

Hua R, Gidda SK, Aranovich A, Mullen RT, Kim PK (2015) Multiple domains in PEX16 mediate its trafficking and recruitment of peroxisomal proteins to the ER. Traffic 16:832–852. https://doi.org/10.1111/tra.12292.

Ito D, Suzuki N (2009) Seipinopathy: a novel endoplasmic reticulum stress-associated disease. Brain 132:8–15. https://doi.org/10.1093/brain/awn216.

Kim KK, Adelstein RS, Kawamoto S (2009) Identification of neuronal nuclei (NeuN) as Fox-3, a new member of the Fox-1 gene family of splicing factors. J Biol Chem 284:31052–31061. https://doi.org/10.1074/jbc.M109.052969.

Kim KK, Nam J, Mukouyama YS, Kawamoto S (2013) Rbfox3-regulated alternative splicing of Numb promotes neuronal differentiation during development. J Cell Biol 200:443–458. https://doi.org/10.1083/jcb.201206146.

Kim PK, Mullen RT (2013) PEX16: a multifaceted regulator of peroxisome biogenesis. Front Physiol 4:241. https://doi.org/10.3389/fphys.2013.00241.

Kim PK, Mullen RT, Schumann U, Lippincott-Schwartz J (2006) The origin and maintenance of mammalian peroxisomes involves a de novo PEX16-dependent pathway from the ER. J Cell Biol 173:521–532. https://doi.org/10.1083/jcb.200601036.

Li G, Zhou L, Zhu Y, Wang C, Sha S, Xian X, Ji Y, Liu G, Chen L (2015) Seipin knockout in mice impairs stem cell proliferation and progenitor cell differentiation in the adult hippocampal dentate gyrus via reduced levels of PPARgamma. Dis Model Mech 8:1615–1624. https://doi.org/10.1242/dmm.021550.

Liu X, Xie B, Qi Y, Du X, Wang S, Zhang Y, Paxinos G, Yang H, Liang H (2016) The expression of SEIPIN in the mouse central nervous system. Brain Struct Funct 221:4111–4127. https://doi.org/10.1007/s00429-015-1151-3.

Livak KJ, Schmittgen TD (2001) Analysis of relative gene expression data using real-time quantitative PCR and the 2(−Delta Delta C (T)) method. Methods 25:402–408. https://doi.org/10.1006/meth.2001.1262.

López-Otín C, Blasco MA, Partridge L, Serrano M, Kroemer G (2013) The hallmarks of aging. Cell 153:1194–1217. https://doi.org/10.1016/j.cell.2013.05.039.

Magre J, Delépine M, Khallouf E, Gedde-Dahl Jr T, Van Maldergem L, Sobel E, Papp J, Meier M, Mégarbané A, Bachy A, et al. (2001) Identification of the gene altered in Berardinelli-Seip congenital lipodystrophy on chromosome 11q13. Nat Genet 28:365–370. https://doi.org/10.1038/ng585.

Nordgren M, Fransen M (2014) Peroxisomal metabolism and oxidative stress. Biochimie 98:56–62. https://doi.org/10.1016/j.biochi.2013.07.026.

Qian Y, Yin J, Hong J, Li G, Zhang B, Liu G, Wan Q, Chen L (2016) Neuronal seipin knockout facilitates Abeta-induced neuroinflammation and neurotoxicity via reduction of PPARgamma in hippocampus of mouse. J Neuroinflammation 13:145. https://doi.org/10.1186/s12974-016-0598-3.

Ruiz-Riquelme A, Sánchez-Iglesias S, Rábano A, Guillén-Navarro E, Domingo-Jiménez R, Ramos A, Rosa I, Senra A, Nilsson P, García Á, et al. (2015) Larger aggregates of mutant seipin in Celia's encephalopathy, a new protein misfolding neurodegenerative disease. Neurobiol Dis 83:44–53. https://doi.org/10.1016/j.nbd.2015.08.006.

Salo VT, Belevich I, Li S, Karhinen L, Vihinen H, Vigouroux C, Magré J, Thiele C, Hölttä-Vuori M, Jokitalo E, Ikonen E (2016) Seipin regulates ER-lipid droplet contacts and cargo delivery. EMBO J 35:2699–2716. https://doi.org/10.15252/embj.201695170.

Santos MJ, Quintanilla RA, Toro A, Grandy R, Dinamarca MC, Godoy JA, Inestrosa NC (2005) Peroxisomal proliferation protects from

β-amyloid neurodegeneration. J Biol Chem 280:41057–41068. https://doi.org/10.1074/jbc.M505160200.

Shai N, Schuldiner M, Zalckvar E (2016) No peroxisome is an island – peroxisome contact sites. Biochim Biophys Acta Mol Cell Biol Lipids 1863:1061–1069. https://doi.org/10.1016/j.bbamcr.2015.09.016.

Sim MF, Talukder MM, Dennis RJ, O'Rahilly S, Edwardson JM, Rochford JJ (2013) Analysis of naturally occurring mutations in the human lipodystrophy protein seipin reveals multiple potential pathogenic mechanisms. Diabetologia 56:2498–2506. https://doi.org/10.1007/s00125-013-3029-3.

Sim MF, Talukder MU, Dennis RJ, Edwardson JM, Rochford JJ (2014) Analyzing the functions and structure of the human lipodystrophy protein seipin. Methods Enzymol 537:161–175. https://doi.org/10.1016/B978-0-12-411619-1.00009-4.

Victoria B, Cabezas-Agrícola JM, González-Méndez B, Lattanzi G, Del Coco R, Loidi L, Barreiro F, Calvo C, Lado-Abeal J, Araújo-Vilar D (2010) Reduced adipogenic gene expression in fibroblasts from a patient with type 2 congenital generalized lipodystrophy. Diabet Med 27:1178–1187. https://doi.org/10.1111/j.1464-5491.2010.03052.x.

Wang H, Becuwe M, Housden BE, Chitraju C, Porras AJ, Graham MM, Liu XN, Thiam AR, Savage DB, Agarwal AK, et al. (2016) Seipin is required for converting nascent to mature lipid droplets. eLife 5. https://doi.org/10.7554/eLife. 16582.

Wang S, Idrissi FZ, Hermansson M, Grippa A, Ejsing CS, Carvalho P (2018) Seipin and the membrane-shaping protein Pex30 cooperate in organelle budding from the endoplasmic reticulum. Nat Commun 9:2939. https://doi.org/10.1038/s41467-018-05278-2.

Zhou L, Chen T, Li G, Wu C, Wang C, Li L, Sha S, Chen L, Liu G, Chen L (2016) Activation of PPARgamma ameliorates spatial cognitive deficits through restoring expression of AMPA receptors in seipin knock-out mice. J Neurosci. 36:1242–1253. https://doi.org/10.1523/JNEUROSCI.3280-15.2016.

(Received 26 May 2018, Accepted 3 November 2018)
(Available online 15 November 2018)